 CMC, vol.29, no.2, pp.169-211, 2012

Development of 3D T-Trefftz Voronoi Cell Finite Elements with/without Spherical Voids &/or Elastic/Rigid Inclusions for Micromechanical Modeling of Heterogeneous Materials

L. Dong[1] **and S. N. Atluri**[1]

Abstract: In this paper, three-dimensionalT-Trefftz Voronoi Cell Finite Elements (VCFEM-TTs) are developed for micromechanical modeling of heterogeneous materials. Several types of VCFEMs are developed, depending on the types of heterogeneity in each element. Each VCFEM can include alternatively a spherical void, a spherical elastic inclusion, a spherical rigid inclusion, or no voids/inclusions at all.In all of these cases, an inter-element compatible displacement field is assumed at each surface of the polyhedral element, with Barycentric coordinates as nodal shape functions.The T-Trefftz trial displacement fields in each element are expressed in terms of the Papkovich-Neuber solution. Spherical harmonics are used as the Papkovich-Neuber potentials to derive the T-Trefftz trial displacement fields. Characteristic lengthsareused for each element to scale the T-Trefftztrial functions, in order to avoid solving systems of ill-conditioned equations. Two approaches for developing element stiffness matrices are used.The differencesbetween these two approachesare that, the compatibilitybetweenthe independentlyassumed fieldsin the interior of the element with those at the outer- as well as the inner-boundary, are enforced alternatively, byLagrange multipliers in multi-fieldboundary variational principles, or by collocation at a finite number of preselected points. These elements are named as VCFEM-TT-BVP and VCFEM-TT-C respectively, following the designations of [Dong and Atluri (2011b, 2012a)].Several three-dimensional computational micromechanics problems are solved using these elements. Computational results demonstrate that both VCFEM-TT-BVP and VCFEM-TT-C can solve three-dimensional problems efficiently and accurately. Especially, these VCFEM-TTs can capture the stress concentration around spherical voids/inclusion quite accurately, and the time for computing each element is much less than that for the hybrid-stress version of VCFEM in [Ghosh and Moorthy (2004)]. Therefore, we consider that the 3D Voronoi Cell Finite Elements developed in this study are suit-

[1] Center for Aerospace Research & Education, University of California, Irvine

able for micromechanical modeling of heterogeneous materials. We also point out-that, the process of reducing ellipsoidal coordinates/harmonics to spherical ones in the limiting case cannot work smoothly, which was contrarily presented in an ambiguous way in [Ghosh and Moorthy (2004)]. VCFEMs with ellipsoidal, and arbitrary shaped voids/inclusions will be presented in future studies.

Keywords: T-Trefftz, VCFEM,matrix, inclusion, void, variational principle, collocation, LBB conditions, completeness, efficiency, Barycentric coordinates, Papkovich-Neuber solution, spherical harmonics

1 Introduction

In recent decades, increasing advancement of science, technology, and the wideapplication of heterogeneous materials, have been experienced in mechanical, aerospace and military industries. For example, metal/alloys with precipitates/pores, and metal/polymer/ceramic composite materials with fiber/whisker/particulate reinforcements are of particular interest. Development of efficient and accurate tools to model the micromechanical and macromechanical behavior of heterogeneous materials is of fundamental importance.

There are several widely-used analytical tools to predict the overall properties of heterogeneous materials. For example, [Hashin and Shtrikman (1963)] developed variational principles to estimate the upper and lower bounds of the elasticity or compliance tensor. [Hill (1965)] developed a self-consistent approach to estimate the homogenized material properties. For a useful reference, one can refer to the book [Nemat-Nasser and Hori (1999)]. Analytical methods have their unique values in the study of micromechanics. However, because most of these methods follow the work of [Eshelby (1957)], namely the elastic field of an ellipsoidal inclusion in an infinite media, it is expected that these methods can only accurately model heterogeneous materials with simple geometries and low volume fractions of inclusions.

The need for predicting the overall properties of a material with complex geometry, distribution, and arbitrary volume fraction of inclusions, promoted the development of computational tools for micromechanics. A popular way of doing this is to use finite elements to model a Representative Volume Element (RVE). By concept, a RVE is a microscopic material volume, which is statistically representative of the infinitesimal material neighborhood of the macroscopic material point of interest. By modeling simple loading cases of the RVE, the microscopic stress field and strain field in the RVE can be computed by the finite element method. And the homogenized material properties are calculated by relating the macroscopic (average) stress tensor to the macroscopic (average) strain tensor. Some useful refer-

ences can be found in [Christman, Needleman and Suresh (1989), Bao, Hutchinson, McMeeking(1991)]. Finite element method and asymptotic homogenization theory were also combined to perform multi-scale modeling of structures composed of heterogeneous materials in [Guedes and Kikuchi (1990)].

However, it is well known that, primal finite elements, which involve displacement-type of nodal shape functions, are highly inefficient for modeling stress concentration problems. Accurate computation of the fields around a single inclusion or void may need thousands of elements. Moreover, meshing of a RVE which contains a large number of inclusions/voids, can be human-labor intensive. For the expensive burden of computation as well as meshing, the above-mentioned computational models mostly use a Unit Cell as the RVE, assuming the microstructure of material is strictly periodic. This obviously cannot account for the complex shape and distribution of materials of different phases.

In order to reduce the burden of computation and meshing, [Ghosh and Mallett (1994); Ghosh, Lee and Moorthy (1995)] proposed the idea of Voronoi Cell Finite Elements (VCFEMs). The RVE is meshed using Voronoi Diagram according to the locations of inclusions/voids, and each Voronoi Cell with/without an inclusion/void can be modeled using one singe finite element. Ghosh's VCFEMs are all developed based the hybrid stress model of [Pian (1964)], using the modified principle of complementary energy, and assuming inter-element compatible displacement fields and a priori equilibrated stress fields. The a priori equilibrated stress fields are generated by using Airy's stress functions in 2D or Maxwell's stress functions in 3D. However, the hybrid stress approach involves Lagrange multipliers, and involves both domain and boundary integration for each and every element. This makes the VCFEMs developed by Ghosh and his coworkers computationally inefficient, and also plagued by LBB conditions. The completeness of the stress fields generated by polynomial Airy's stress functions or Maxwell's stress functions is also of obvious questionability. Incomplete stress field assumptions lead to very poor results of computed stress/strain fields. Attempts were made to improve the accuracy by introducing additional stress fields. For example, in the 3D VCFEMs developed by [Ghosh and Moorthy (2004)], the analytical stress field around an ellipsoidal inclusion embedded in an infinite media subjected to remote loads was added to the stress field generated by the polynomial Maxwell's stress functions. However, the stress fieldis still not necessarily complete, even though some improvement was made by introducing this additional stress field. For detailed discussion of completeness, see [Muskhelishvili (1954)] for 2D problems, and [Lurie (2005)] for 3D problems.

In order to overcome the several aforementioned disadvantages, a different class of VCFEMs wasdeveloped recently by the authors—T-Treffz Voronoi Cell Finite Ele-

ments (VCFEM-TTs), which are efficient and accurate for micromechanical modeling of heterogeneous materials. Two-dimensional cases of VCFEM-TTs were presented in [Dong and Atluri(2011b);Dong and Atluri(2012a)]. The main difference of VCFEM-TTs developed by the authors and the VCFEMs developed by Ghosh and his coworkers is that: a complete T-Trefftz trial displacement field which satisfies both equilibrium and compatibility is assumed in VCFEM-TTs, instead of only the "a priori equilibrated" stress field used in [Ghosh, Lee and Moorthy (1995)]. VCFEM-TTs developed by the authors are computationally more efficient, because only boundary integrals are needed in VCFEM-TTs, instead of both the volume and surface integrals needed in the hybrid-stress elements developed by Ghosh et al. VCFEM-TT-C, one of the two classes of VCFEM-TTs developed by the authors, is not plagued by LBB conditions, because no Lagrange multipliers are involved. VCFEM-TTs can also model the stress concentration around voids/inclusions much more accurately, because of the completeness of the T-Trefftz trial displacement fields, see [Dong and Atluri (2012b)].

In this study, we extend VCFEM-TTs to solve 3D problems. 3D VCFEM-TTs without voids/inclusions, with a spherical void, with a spherical elastic inclusion, or with a spherical rigid inclusion are developed respectively. The inter-element displacement field is assumed by using Barycentric coordinates as nodal shape functions. The T-Trefftz trial displacement fields are assumed in the form of Papkovich-Neuber solutions. Spherical harmonics are used as Papkovich-Neuber potentials. Two approaches for developing element stiffness matrices are used. The compatibility betweenthe independently assumed fields at the outer- as well as the inner-boundary, are enforced alternatively, by Lagrange multipliers in multi-field boundary variational principles, or by collocation at a finite number of preselected points. These elements are named as VCFEM-TT-BVP and VCFEM-TT-C respectively. Numerical experiments using elements without inclusions and with spherical inclusions show high-performance of the developed VCFEM-TTs.

The rest of this paper is organized as follows: in section 2, we use Barycentric coordinates to develop the inter-element compatible displacement field; in section 3, we introduce the T-Trefftz trial displacement fields in the form of Papkovich-Neuber solution; in section 4, we briefly discuss spherical harmonics asPapkovich-Neuber potentials; in section 5, we develop and test the performance of 3D VCFEM-TTs without voids/inclusions; in section 6, we develop and test the performance of 3D VCFEM-TTs with spherical voids/inclusions; in section 7, we complete this paper with some concluding remarks.

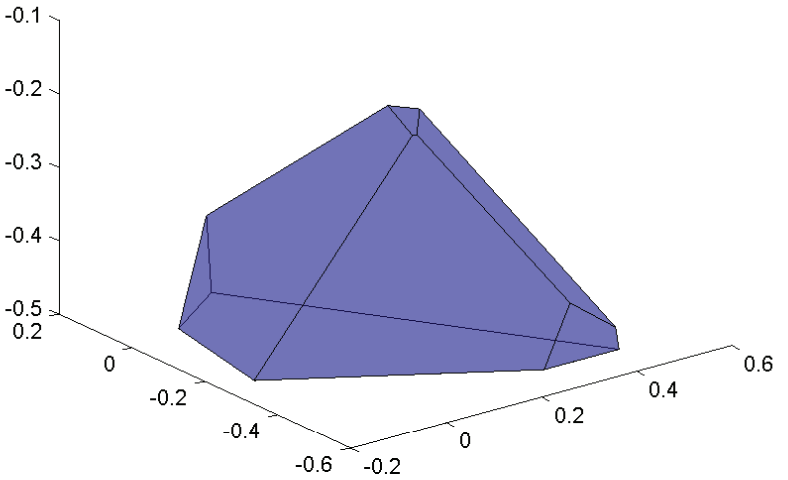

Figure 1: A 3D Voronoi Cell Finite Element

2 Boundary Displacement Fields with Barycentric Coordinates as Nodal Shape Functions

For an arbitrary VCFEM in the 3D space,each surface is a polygon, see Fig. 1 for example. Constructing an inter-element compatible displacement on the boundary of the polyhedral element is not as simple as that for 2D VCFEMs. One way of doing this is to use Barycentric coordinates as nodal shape functions on each polygonal face of the 3D VCFEM.

Consider a polygon face V_n with n nodes $\mathbf{x}^1$, $\mathbf{x}^2$,... $\mathbf{x}^n$, the Barycentric coordinates, denoted as $\lambda_i (i = 1, 2, ... n)$. λ_i is only a function of the position vector $\mathbf{x}$. To obtain a good performance of VCFEM, we only consider Barycentric coordinates which satisfy the following properties:

1. Non-negative: $\lambda_i \geq 0$ in the polygon V_n
2. Smooth: λ_i is at least C^1 continuous in the polygon V_n
3. Linear along each edge that composes the polygon V_n

4. Linear completeness: For any linear function $f(\mathbf{x})$, the following equality holds: $f(\mathbf{x}) = \sum_{i=1}^{n} f(\mathbf{x^i})\lambda_i$
5. Partition of unity: $\sum_{i=1}^{n} \lambda_i \equiv 1$.
6. Dirac delta property: $\lambda_i(\mathbf{x^j}) = \delta_{ij}$.

Among the many Barycentric coordinates that satisfy these conditions, Wachspress coordinates [Wachspress (1975)] is among the most simple and efficient.

Let $\mathbf{x} \in V_n$, and define the areas: $B_i$as the area of the triangle with$\mathbf{x^{i-1}}, \mathbf{x^i}$ and $\mathbf{x^{i+1}}$ as its three vertices, and $A_i(\mathbf{x})$ as the area of the triangle having $\mathbf{x}$, $\mathbf{x^i}$ and $\mathbf{x^{i+1}}$ as its three vertices. This is illustrated in Fig. 2.

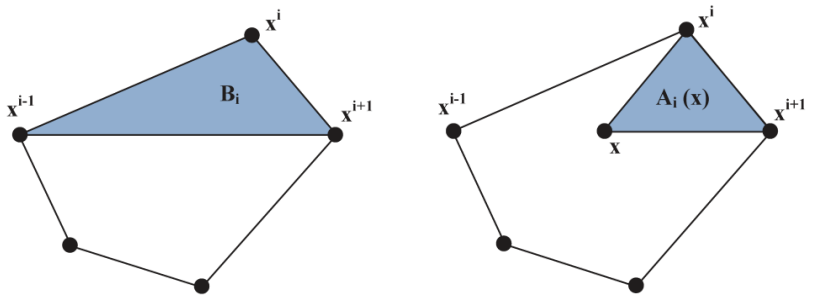

Figure 2: Definition of triangles B_i and $A_i(\mathbf{x})$

Define the Wachspress weight function as:

$$w_i(\mathbf{x}) = B_i \prod_{j \neq i, i-1} A_j(\mathbf{x}) \tag{1}$$

Then, the Wachspress coordinates are given by the rational functions:

$$\lambda_i(\mathbf{x}) = \frac{w_i(\mathbf{x})}{\sum_{j=1}^{n} w_j(\mathbf{x})} \tag{2}$$

Fig. 3 shows the Wachspress coordinate for one node of a regular pentagon. It can be seen that the Wachspress coordinate as shown in Fig. 3 have all the properties described previously in this section.

Similar to the well-known triangular Barycentric coordinates used in the 2D primal triangular elements, the nodal shape functions associated with the vertices of this

polygonal surface displacement field are their corresponding Barycentric coordinates. An inter-element compatible displacement field is therefore expressed in the following form:

$$\tilde{u}_i(\mathbf{x}) = \sum_{k=1}^{n} \lambda_k(\mathbf{x})\, u_i(\mathbf{x}^k) \quad \mathbf{x} \in V_n, V_n \subset \partial\Omega^e \tag{3}$$

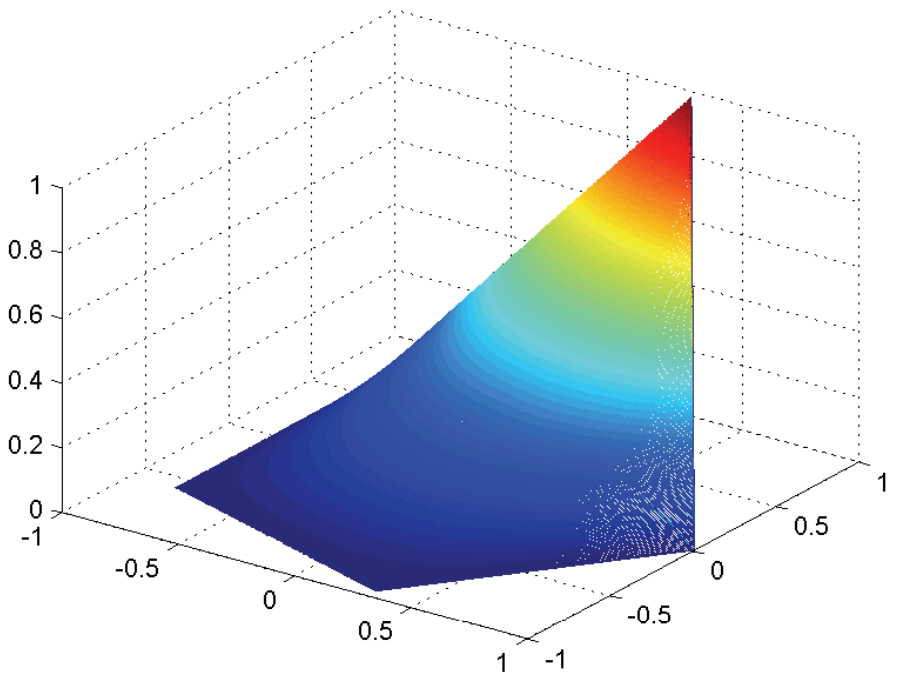

Figure 3: Barycentric coordinates as nodal shape functions

3 T-Trefftz Trial Displacement field: the Papkovich-Neuber Solution

Consider a linear elastic solid undergoing infinitesimal elasto-static deformation. Cartesian coordinates x_i identify material particles in the solid. $\sigma_{ij}, \varepsilon_{ij}, u_i$ are Cartesian components of the stress tensor, strain tensor and displacement vector respectively. $\overline{f}_i, \overline{u}_i, \overline{t}_i$ are Cartesian components of the prescribed body force, boundary

displacement and boundary traction vector. S_u, S_t are displacement boundary and traction boundary of the domain Ω. We use $()_{,i}$to denote differentiation with respect to x_i. The equations of linear and angular momentum balance, constitutive equations, compatibility equations, and boundary conditions can be written as:

$$\sigma_{ij,j} + \overline{f}_i = 0 \text{ in } \Omega \tag{4}$$

$$\sigma_{ij} = \sigma_{ji} \text{ in } \Omega \tag{5}$$

$$\sigma_{ij} = C_{ijkl}\varepsilon_{kl} \text{ (or } \varepsilon_{ij} = S_{ijkl}\sigma_{kl}) \text{ in } \Omega \text{ for a linear elastic solid} \tag{6}$$

$$\varepsilon_{ij} = \frac{1}{2}(u_{i,j} + u_{j,i}) \equiv u_{(i,j)} \text{ in } \Omega \tag{7}$$

$$u_i = \overline{u}_i \text{ at } S_u \tag{8}$$

$$n_j\sigma_{ij} = \overline{t}_i \text{ at } S_t \tag{9}$$

For 3D isotropic media where body force is negligible, equation (4)-(6) can be rewritten in terms of displacements, which is the Navier's equation:

$$(\lambda + \mu)\theta_{,i} + \mu\Delta u_i = 0 \tag{10}$$

where

$$\begin{aligned} \theta &= u_{k,k} \\ \lambda &= \frac{Ev}{(1+v)(1-2v)} \\ \mu &= G = \frac{E}{2(1+v)} \end{aligned} \tag{11}$$

The T-Trefftz methods start by selecting a set of trial functions which satisfy(10) a priori. For 3D isotropic elasticity, this can be done by using the Papkovich-Neuber solution, see [Lurie (2005)]:

$$\begin{aligned} \mathbf{u} &= \left[4(1-v)\mathbf{B} - \nabla(\mathbf{R}\cdot\mathbf{B} + \mathbf{B_0})\right]/2G \\ &= \left[(3-4v)\mathbf{B} - \mathbf{R}\cdot(\nabla\mathbf{B})^T - \nabla\mathbf{B_0})\right]/2G \end{aligned} \tag{12}$$

$B_0, \mathbf{B}$ are scalar and vector harmonic functions, which are sometimes called Papkovich-Neuber potentials

The second equation in (12) can be written in the following index form:

$$u_i = \left[(3-4v)B_i - x_k B_{k,i} - B_{0,i}\right]/2G \tag{13}$$

An interesting fact of 3D Papkovich-Neuber solution is that, the 3D displacements as in (13) have a very similar form to the displacements in 2D expressed in terms of complex potentials, as shown in [Muskhelishvili (1954)]. However, unlike theapproach of complex potentials, for a specific displacement field u_i in 3D, the harmonic potentials have large degrees of freedom. That is to say, there may exist many different sets of B_0, B_1, B_2, B_3, which are harmonic potentials of the same specific displacement fieldu_i. This prompts people to think about whether it is possible to drop the scalar harmonic function, to express the solution as:

$$\mathbf{u} = [4(1-v)\mathbf{B} - \nabla\mathbf{R}\cdot\mathbf{B}]/2G \tag{14}$$

It was proved by M.G. Slobodyansky that (14) is complete for the infinite region which is external to a closed surface for any v. However, for a simply-connected domain, (14) is complete only when $v \neq 0.25$.

By expressing B_0 to be a specific function of $\mathbf{B}$, M.G. Slobodyansky has shown that a specific case of the Papkovich Neuber solution is :

$$\mathbf{u} = [4(1-v)\mathbf{B} + \mathbf{R}\cdot\nabla\mathbf{B} - \mathbf{R}\nabla\cdot\mathbf{B})]/2G \tag{15}$$

whichis complete for a simply connected domain, for any v.

For detailed discussion of the completeness of the Papkovich-Neuber solution, see [Lurie (2005)].

4 On Spherical Harmonics as Papkovich-Neuber General Potentials

In this section, we make a short introduction to spherical harmonics. One can refer to the monograph [Hobson (1931)] for detailed discussion.

Consider Cartesian coordinates x_1, x_2, x_3 and spherical coordinates $q^1 = R, q^2 = \theta, q^3 = \phi$, related by:

$$\begin{aligned} x_1 &= R\sin\theta\cos\phi \\ x_2 &= R\sin\theta\sin\phi \\ x_3 &= R\cos\theta \end{aligned} \tag{16}$$

We use $\mathbf{e}_i$ to denote base vectors of the Cartesian coordinate system, and $\mathbf{R} = x_i\mathbf{e}_i$ to denote the position vector. From (16) we have:

$$\begin{aligned} &\frac{\partial x_1}{\partial R} = \sin\theta\cos\phi, \quad \frac{\partial x_1}{\partial \theta} = R\cos\theta\cos\phi, \quad \frac{\partial x_1}{\partial \phi} = -R\sin\theta\sin\phi, \\ &\frac{\partial x_2}{\partial R} = \sin\theta\sin\phi, \quad \frac{\partial x_2}{\partial \theta} = R\cos\theta\sin\phi, \quad \frac{\partial x_2}{\partial \phi} = R\sin\theta\cos\phi, \\ &\frac{\partial x_3}{\partial R} = \cos\theta, \quad \frac{\partial x_3}{\partial \theta} = -R\sin\theta, \quad \frac{\partial x_3}{\partial \phi} = 0. \end{aligned} \tag{17}$$

And

$$\begin{aligned} &\frac{\partial q^s}{\partial x_k} = \frac{1}{H_s^2}\frac{\partial x_k}{\partial q^s} \\ &\frac{\partial \mathbf{R}}{\partial q^r}\cdot\frac{\partial \mathbf{R}}{\partial q^s} = \delta_{rs}H_r H_s \end{aligned} \tag{18}$$

where

$$\begin{aligned} &H_1 = H_R = 1 \\ &H_2 = H_\theta = R \\ &H_3 = H_\phi = R\sin\theta \end{aligned} \tag{19}$$

are called Lame's coefficients. By defining a set of orthonormal base vectors of the spherical coordinate system:

$$\mathbf{g}_r = \frac{1}{H_r}\frac{\partial \mathbf{R}}{\partial q^r} \tag{20}$$

we have:

$$\begin{aligned} &\frac{\partial \mathbf{g}_R}{\partial R} = 0, \quad \frac{\partial \mathbf{g}_R}{\partial \theta} = \mathbf{g}_\theta, \quad \frac{\partial \mathbf{g}_R}{\partial \phi} = \mathbf{g}_\phi \sin\theta, \\ &\frac{\partial \mathbf{g}_\theta}{\partial R} = 0, \quad \frac{\partial \mathbf{g}_\theta}{\partial \theta} = -\mathbf{g}_R, \quad \frac{\partial \mathbf{g}_\theta}{\partial \phi} = \mathbf{g}_\phi \cos\theta, \\ &\frac{\partial \mathbf{g}_\phi}{\partial R} = 0, \quad \frac{\partial \mathbf{g}_\phi}{\partial \theta} = 0, \quad \frac{\partial \mathbf{g}_\phi}{\partial \phi} = -\left(\mathbf{g}_R \sin\theta + \mathbf{g}_\theta \sin\theta\right), \end{aligned} \tag{21}$$

Therefore, the Laplace operator of a scalar λ has the following form:

$$\begin{aligned} &\nabla^2\lambda = \nabla\cdot\nabla\lambda = \frac{1}{H_r}\mathbf{g}_r\frac{\partial}{\partial q_r}\cdot\frac{1}{H_s}\mathbf{g}_\mathbf{s}\frac{\partial \lambda}{\partial q_s} \\ &= \frac{1}{R}\left[\frac{\partial}{\partial R}R^2\frac{\partial \lambda}{\partial R} + \frac{\partial}{\partial \mu}(1-\mu^2)\frac{\partial \lambda}{\partial \mu} + \frac{1}{1-\mu^2}\frac{\partial \lambda}{\partial \lambda^2}\right] \end{aligned} \tag{22}$$

where the new variable $\mu = \cos\theta$ is introduced.

By separating of variables, assuming $\lambda = L(R)M(\mu)N(\phi)$ and using m^2 and $n(n+1)$ as separating constants, it can be shown that L, M, N should satisfy the following equations:

$$N''(\phi) + m^2 N(\phi) = 0 \tag{23}$$

$$\left[(1-\mu^2)M'(\mu)\right]' + \left[n(n+1) - \frac{m^2}{1-\mu^2}\right]M(\mu) = 0 \tag{24}$$

$$\left[R^2L'(R)\right]' - n(n+1)L(R) = 0 \tag{25}$$

Equation (23) leads to particular solutions $\cos m\phi$ and $\sin m\phi$ for an non-negative integer m, because we require $N(\phi)$ to be periodic, with 2π as the period.

Equations (24), which is obviously the associated Legendre's differential equation, leads to associated Legendre's functions of the first and the second kind. Because the latter is singular at poles $\mu = \pm 1$, only the associated Legendre's functions of the first kind are valid for constructing $M(\mu)$. Denoting them as $P_n^m(\mu)$, we have:

$$\begin{aligned} P_n^m(\mu) &= (-1)^m(1-\mu^2)^{m/2}\frac{d^m}{d\mu^m}P_n(\mu) \\ P_n(\mu) &= \frac{1}{2^2 n!}\left[\frac{d^n}{d\mu^n}(\mu^2-1)^n\right] \end{aligned} \tag{26}$$

The product of $M(\mu)N(\phi)$ are called spherical surface harmonics. And it can be normalized to be:

$$\begin{aligned} Y_n^m(\theta,\phi) &= \sqrt{\frac{2n+1}{4\pi}\frac{(n-m)!}{(n+m)!}}P_n^m(\cos(\theta))e^{im\phi} \\ &= \sqrt{\frac{2n+1}{4\pi}\frac{(n-m)!}{(n+m)!}}P_n^m(\cos(\theta))\left[\cos(m\phi)+i\sin(m\phi)\right] \\ &= YC_n^m(\theta,\phi) + iYS_n^m(\theta,\phi) \end{aligned} \tag{27}$$

such that

$$\int_0^{2\pi}\int_0^{\pi} Y_n^m(\theta,\phi)\bar{Y}_{n'}^{m'}(\theta,\phi)\sin\theta d\theta d\phi = \delta_{mm'}\delta_{nn'} \tag{28}$$

Finally, Eq. (25) leads to particular solutions R^n and $R^{-(n+1)}$. For different problems, different forms of $L(R)$ should be used, which leads to different forms of spherical harmonics. For the internal problem of a sphere, only R^n is valid. λcan be expanded as:

$$\lambda_p = \sum_{n=0}^{\infty} R^n \left\{ a_0^0 YC_0^0(\theta,\phi) + \sum_{m=1}^{n}\left[a_n^m YC_n^m(\theta,\phi) + b_n^m YS_n^m(\theta,\phi)\right]\right\} \tag{29}$$

For external problems in an infinite domain, only $R^{-(n+1)}$ is valid, λ can be expanded as:

$$\lambda_k = \sum_{n=0}^{\infty} R^{-(n+1)} \left\{ c_0^0 YC_0^0(\theta,\phi) + \sum_{m=1}^{n}\left[c_n^m YC_n^m(\theta,\phi) + d_n^m YS_n^m(\theta,\phi)\right]\right\} \tag{30}$$

For external problems in a finite domain, a hollow sphere for instance, λ is the summation of (29)(30):

$$\begin{aligned}\lambda_p+\lambda_k=&\sum_{n=0}^{\infty}R^n\left\{a_0^0YC_0^0(\theta,\phi)+\sum_{m=1}^{n}\left[a_n^mYC_n^m(\theta,\phi)+b_n^mYS_n^m(\theta,\phi)\right]\right\}\\&+\sum_{n=0}^{\infty}R^{-(n+1)}\left\{c_0^0YC_0^0(\theta,\phi)+\sum_{m=1}^{n}\left[c_n^mYC_n^m(\theta,\phi)+d_n^mYS_n^m(\theta,\phi)\right]\right\}\end{aligned}\tag{31}$$

However, these assumptions of trial functions will lead to ill-conditioned systems of equations when being applied in Trefftz method to numerically solve a boundary value problem. We use characteristic lengths which was introduced in [Liu (2007a,b)] to scale the T-Trefftz trial functions.

For a specific domain of interest, two characteristic lengths R_p and R_k are defined, which are respectively the maximum and minimum values of radial distance R of points where boundary conditions are specified. Therefore, $\left(\frac{R}{R_p}\right)^n$ and $\left(\frac{R_k}{R}\right)^{-(n+1)}$ is confined between 0 and 1 for any positive integer$n$. Harmonics are thereafter scaled as:

$$\begin{aligned}\lambda_p=&\sum_{n=0}^{\infty}\left(\frac{R}{R_p}\right)^n\left\{a_0^0YC_0^0(\theta,\phi)+\sum_{m=1}^{n}\left[a_n^mYC_n^m(\theta,\phi)+b_n^mYS_n^m(\theta,\phi)\right]\right\}\\\lambda_k=&\sum_{n=0}^{\infty}\left(\frac{R}{R_k}\right)^{-(n+1)}\left\{c_0^0YC_0^0(\theta,\phi)+\sum_{m=1}^{n}\left[c_n^mYC_n^m(\theta,\phi)+d_n^mYS_n^m(\theta,\phi)\right]\right\}\end{aligned}\tag{32}$$

5 T-Trefftz VCFEMs without Inclusions/Voids

5.1 Basic Theory and Formulation

For an element with N nodes, the displacement along each polygonal surface is assumed using Wachspress coordinates as nodal shape functions:

$$\tilde{\mathbf{u}}=\tilde{\mathbf{N}}\mathbf{q}\ \text{ at } \partial\Omega^e \tag{33}$$

An interior displacement field is also independently assumed using the Papkovich-Neuber Solution. Without inclusions or voids, the element is a simply-connected domain. Therefore, the source point is put at the center, and the Papkovich-Neuber displacement potentials are expressed as:

$$\mathbf{B}=\sum_{n=0}^{M}\left(\frac{R}{R_c}\right)^n\left\{\mathbf{a}_0^0YC_0^0(\theta,\phi)+\sum_{m=1}^{n}\left[\mathbf{a}_n^mYC_n^m(\theta,\phi)+\mathbf{b}_n^mYS_n^m(\theta,\phi)\right]\right\} \tag{34}$$

R_c is the characteristic length used to scale the T-Trefftz trial functions, in order to avoid solving ill-conditioned systems of equations. $R_c$should be the largest distance between the source point, and any point along the element boundary.

It should be pointed out, that although each component of the harmonic vector of $\mathbf{B}$ is expressed in terms of spherical coordinates, these spherical harmonics of each order n are actually homogenous polynomials of x_1, x_2, x_3 of the same order n. Therefore, such a displacement field does not impose any difficulty for numerical integration.

And the T-Trefftz trial dispacelement field is expressed as:

$$\mathbf{u} = \left[4(1-\nu)\mathbf{B} + \mathbf{R}\cdot\nabla\mathbf{B} - \mathbf{R}\nabla\cdot\mathbf{B})\right]/2G \tag{35}$$

We point out that displacement field assumed in this way is rotationally invariant.

We also list the 6 modes which corresponds to the six rigid body modes in 3D. They are:

$$\begin{aligned}
&\mathbf{a}_0^0 = \begin{Bmatrix}1 & 0 & 0\end{Bmatrix}^T \\
&\mathbf{a}_0^0 = \begin{Bmatrix}0 & 1 & 0\end{Bmatrix}^T \\
&\mathbf{a}_0^0 = \begin{Bmatrix}0 & 0 & 1\end{Bmatrix}^T \\
&\mathbf{a}_1^0 = \begin{Bmatrix}1 & 0 & 0\end{Bmatrix}^T, \quad \mathbf{a}_1^1 = \begin{Bmatrix}0 & 0 & \sqrt{2}\end{Bmatrix}^T \\
&\mathbf{a}_1^0 = \begin{Bmatrix}0 & 1 & 0\end{Bmatrix}^T, \quad \mathbf{a}_1^1 = \begin{Bmatrix}0 & \sqrt{2} & 0\end{Bmatrix}^T \\
&\mathbf{a}_1^1 = \begin{Bmatrix}0 & 1 & 0\end{Bmatrix}^T, \quad \mathbf{b}_1^1 = \begin{Bmatrix}-1 & 0 & 0\end{Bmatrix}^T
\end{aligned} \tag{36}$$

Whether these modes need to be removed or not, beforehand, depends on how the element stiffness matrix is developed.

In principle, for a VCFEM with N nodes, the truncation order M should be no smaller than $\lceil\sqrt{N}\rceil - 1$, so that non-rigid body modes included in u_i is equal or larger than $3N-6$, the number of non-rigid-body modes included in $\tilde{u}_i$. $\lceil\sqrt{N}\rceil$ is the smallest integer which is equal or larger than $\sqrt{N}$. However, based on some numerical examples, it was found that $M = \lceil\sqrt{N}\rceil$ is a good option. In this study, such an order truncation is always used.

Adopting matrix and vector notation, we have:

$$\begin{aligned}
&\mathbf{u} = \mathbf{N}\boldsymbol{\alpha} \text{ in } \Omega^e \\
&\boldsymbol{\varepsilon} = \mathbf{B}\mathbf{q} \text{ in } \Omega^e \\
&\boldsymbol{\sigma} = \mathbf{D}\boldsymbol{\varepsilon} = \mathbf{P}\alpha \text{ in } \Omega^e \\
&\mathbf{t} = \mathbf{n}\boldsymbol{\sigma} = \mathbf{R}\boldsymbol{\alpha} \text{ at } \partial\Omega^e
\end{aligned} \tag{37}$$

Firstly, we can substitute the assumed $u_i, \tilde{u}_i$ into a two-field boundary variational principle:

$$\pi_1(u_i,\tilde{u}_i) = \sum_e \left\{ \int_{\Omega^e} \frac{1}{2} t_i u_i dS - \int_{\partial\Omega^e} t_i \tilde{u}_i dS + \int_{S_t^e} \bar{t}_i \tilde{u}_i dS \right\} \tag{38}$$

Substituting assumed $u_i, \tilde{u}_i$ into the boundary variational principle (38), we have:

$$\begin{aligned} &\delta\pi_1(\boldsymbol{\alpha},\mathbf{q}) = 0 \\ &= \delta \sum_e \left(\frac{1}{2}\boldsymbol{\alpha}^T \mathbf{H}\boldsymbol{\alpha} - \mathbf{q}^T \mathbf{G}^T \boldsymbol{\alpha} + \mathbf{q}^T \mathbf{Q} \right) \\ &= \sum_e \left(\delta\boldsymbol{\alpha}^T \mathbf{H}\boldsymbol{\alpha} - \delta\mathbf{q}^T \mathbf{G}^T \boldsymbol{\alpha} - \delta\boldsymbol{\alpha}^T \mathbf{G}\mathbf{q} + \delta\mathbf{q}^T \mathbf{Q} \right) \end{aligned} \tag{39}$$

where

$$\begin{aligned} \mathbf{G} &= \int_{\partial\Omega^e} \mathbf{R}^T \tilde{\mathbf{N}} dS \\ \mathbf{H} &= \int_{\partial\Omega^e} \mathbf{R}^T \mathbf{N} dS \\ \mathbf{Q} &= \int_{S_t^e} \tilde{\mathbf{N}}^T \bar{\mathbf{t}} dS \end{aligned} \tag{40}$$

Finite element equations derived in this way are:

$$\sum_e \left(\delta\mathbf{q}^T \mathbf{K}\mathbf{q} - \delta\mathbf{q}^T \mathbf{Q} \right) = \sum_e \left(\delta\mathbf{q}^T \mathbf{G}^T \mathbf{H}^{-1} \mathbf{G}\mathbf{q} - \delta\mathbf{q}^T \mathbf{Q} \right) = 0 \tag{41}$$

For this case, rigid-body modes should be eliminated from the assumedu_i.

We denote this type of VCFEM as VCFEM-TT-BVP. The development of stiffness matrices of VCFEM-TT-BVP needs integration merely along the boundary. This saves a large amount of computational burden for 3D problems, because domain integration in 3D is computationally intensive. However, VCFEM-TT-BVP is clearly plagued by LBB conditions, because the multi-field boundary variational principle (38) involves Lagrange multipliers. Similarly, because the VCFEMs developed by Ghosh and his coworkers involve Lagrange multipliers, they are also plagued by LBB conditions. Moreover, the VCFEMs developed by Ghosh and his coworkers are based on Hybrid-Stress variational principle of Pian, and involve only equilibrated stresses which are forced to satisfy compatibility conditions through the variational principles. Thus the hybrid-stress VCFEMs of Ghosh et al. involve volume integrals as wells as surface integrals in the development of the VCFEM stiffness matrices. Inability to satisfy LBB conditions will cause the instability of finite elements solutions. For detailed discussion of LBB conditions, see [Babuska (1973);

Brezzi (1974); Rubinstein, Punch and Atluri (1983); Punch and Atluri (1984); Xue, Karlovitz and Atluri (1985)].

A simple approach to develop hybrid/mixed elements without LBB conditions were presented in [Dong and Atluri (2011a)]. The essential idea was to enforce the compatibility between independently assumed fields, using collocation or the least squares method, instead of using Lagrange multipliers in multi-field variational principles. Following this idea, we can also enforce the compatibility of u_i and $\tilde{u}_i$ at a set of preselected collocation points $x_i^{(k)}, k = 1,2...M$ along $\partial\Omega^e$, similar to the procedure of developing 2D VCFEM-TT-C. We obtain:

$$u_i(x_i^{(k)}, \boldsymbol{\alpha}) = \tilde{u}_i(x_i^{(k)}, \mathbf{q}),\ k = 1,2,... \tag{42}$$

A system of linear equations would be obtained:

$$\mathbf{A}\alpha = \mathbf{Bq} \tag{43}$$

In general, (43) is an over-determined system of equations, its solution can be obtained in a least square sense:

$$\alpha = \left(\mathbf{A^T WA}\right)^{-1} \mathbf{A^T WBq} = \mathbf{Cq} \tag{44}$$

wherethe weight matrix $\mathbf{W}$ has only non-zero entries w_k in the diagonal.Each w_k represents the relative weight of the corresponding equation. In this study, each polygonal surface is divided into triangles for the numerical integrations of (40). The collocation points are selected at the integration points of each triangle.And the corresponding w_k is the product of the Jacobian (area of the triangle) and the weight for numerical integration, at each collocation/integration points. With this choice of collocation points and weights, it is obvious that, if a large number of collocation points are used, (44) is equivalent to solving the least square problem of minimizing $\int_{\partial\Omega^e}(u_i - \tilde{u}_i)^2 dS$. However, ensuring the solvability of (44) needs less collocation/integration points than that are needed for exactly integrating $\int_{\partial\Omega^e}(u_i - \tilde{u}_i)^2 dS$, and thus it involves less computational burden.

It should be noted that, using collocation method, the rigid body modes should not be eliminated from the assumedu_i.

In this case, u_i already satisfy governing Navier's equation (10), and are related to $\tilde{u}_i$ using collocation method, which satisfies the inter-element compatibility condition, we can develop finite elements using the following variation principle:

$$\pi_2(u_i) = \sum_e \left\{ \int_{\Omega^e} \frac{1}{2} t_i u_i dS - \int_{S_i^e} \bar{t}_i u_i dS \right\} \tag{45}$$

Substituting the displacement field into (45), we obtain finite element equations:

$$\sum_e \left(\delta \mathbf{q}^T \mathbf{K}\mathbf{q} - \delta \mathbf{q}^T \mathbf{Q}\right) = \sum_e \left(\delta \mathbf{q}^T \mathbf{C}^T \mathbf{H}\mathbf{C}\mathbf{q} - \delta \mathbf{q}^T \mathbf{Q}\right) = 0 \tag{46}$$

We still denote this type of element as VCFEM-TT-C. Because the variational principle (45) does not involve Lagrange multipliers, VCFEM-TT-C is not plagued by LBB conditions.

5.2 Numerical Examples

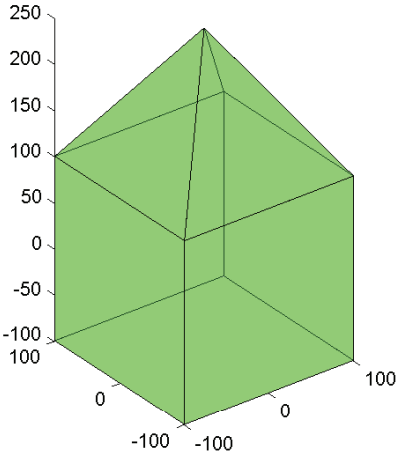

Figure 4: A polyhedron element

Firstly, we illustrate the reason why we use a characteristic length to scale the T-Trefftz trial functions. Material properties$E = 1$ and $\nu = 0.25$ are used. A 3D VCFEM is used, see Fig. 4. We compute the condition number of the coefficient matrices of the equations used to relate $\alpha$to $\mathbf{q}$. Numerical results are shown in Tab.1. We can clearly see that by scaling the T-complete functions, the resulting systems of equations have significantly smaller condition number. In the following examples, the characteristic length is always used to scale the T-Trefftz trial functions.

We also compare the CPU time required for computing the stiffness matrix of the element shown in Fig. 4, using different VCFEM-TTs. The CPU time required

Table 1: Condition number of coefficient matrices of equations used to relate $\boldsymbol{\alpha}$ to $\mathbf{q}$

Elements	VCFEM-TT-BVP		VCFEM-TT-C	
Characteristic length	Scaled	Not Scaled	Scaled	Not Scaled
Condition number	83.4	3.5×10^{12}	350.6	1.6×10^{14}

is shown in Tab. 2. As can be seen, VCFEM-TT-C and VCFEM-TT-BVP need about the same time for computing one element. We would like to point out that, this computational time should be much less than VCFEMs developed in [Ghosh and Moorthy (2004)], even though an non-optimized MATLAB code is used in this study. In [Ghosh and Moorthy (2004)], it was reported that the computational burden for 3D VCFEMs are so high that parallel–processing has to be used to accelerate the computation. However, even for VCFEM-TTs with inclusions/voids developed in this study, the CPU time needed for computing one element is always smaller than 2.5 seconds.

Table 2: CPU time required for computing the stiffness matrix of the element in Fig. 4

CPU Time (second)	VCFEM-TT-BVP	VCFEM-TT-C
	0.71	0.70

Using the same element, we compute the eigenvalues of element stiffness matrices of different VCFEMs. This is conducted in the original and rotated global Cartesian coordinate system. The eigenvalues obviously are invariant with respect to the global coordinate system. Experimental results are recorded in Tab. 3.

As can clearly be seen, these elements are stable and invariant for this shape. However, this does not mean that LBB conditions are satisfied by VCFEM-TT-BVP for an arbitrary element. On this point, VCFEM-TT-C, which does not involve LBB conditions, demonstrates significant advantages.

We also conduct the one-element patch test. The same element in Fig. 4 is used. A uniform traction is applied to the upper faces. The displacements in the lower face are prescribed to be the exact solution. The exact solution is:

$$\begin{aligned} u_1 &= -\frac{P\nu}{E}x_1 \\ u_2 &= -\frac{P\nu}{E}x_2 \\ u_3 &= \frac{P}{E}x_3 \end{aligned} \tag{47}$$

Table 3: Eigenvalues of stiffness matrices of different VCFEMs

Eigenvalues Rotation=0˚&45˚	VCFEM-TT-BVP	VCFEM-TT-C
1	2.3383	2.3454
2	1.0878	1.1019
3	1.0805	1.0907
4	0.8408	0.8436
5	0.8408	0.8436
6	0.8348	0.7706
7	0.6265	0.6167
8	0.6161	0.6055
9	0.6002	0.6014
10	0.6002	0.6014
11	0.5529	0.5372
12	0.5407	0.5297
13	0.5407	0.5297
14	0.5029	0.5042
15	0.2984	0.2972
16	0.2511	0.2551
17	0.2511	0.2551
18	0.1915	0.1835
19	0.1915	0.1835
20	0.1692	0.1740
21	0.1219	0.1323
22	0.0000	0.0000
23	0.0000	0.0000
24	0.0000	0.0000
25	0.0000	0.0000
26	0.0000	0.0000
27	0.0000	0.0000

The numerical result of different elements is shown in Tab. 4, with error defined as:

$$Error = \frac{\|\mathbf{q} - \mathbf{q}^{exact}\|}{\|\mathbf{q}^{exact}\|} \tag{48}$$

VCFEM-TT-BVP can pass the patch test. The numerical error for VCFEM-TT-C is very small.

We also evaluate the performance of VCFEMs by modeling the cantilever beam

Table 4: Performances of different VCFEMs in the constant strain patch test

Error	VCFEM-TT-BVP	VCFEM-TT-C
	5.8×10^{-10}	5.5×10^{-3}

with mesh configuration shown in Fig. 5, and compare their performances to the exact solution. Geometry properties length $L = 10$, width $2c = 2$, depth $2e = 2$. Material properties $E = 1500$ and $v = 0.25$ are used. An end bending moment is applied to the right face with$M = 4000$. The mesh configuration includes 10 elements, as shown in Fig. 5. Traction boundary conditions are applied to the right side of the beam. The displacements on the left side are prescribed to be the exact solution. The exact solutions can be found in [Timoshenko and Goodier (1970)]. Computed tip vertical displacement at point A, and normal stress at point B are shown in Tab. 5. From this example, we can see that similar accuracies can be obtained by VCFEM-TT-BVP and VCFEM-TT-C.

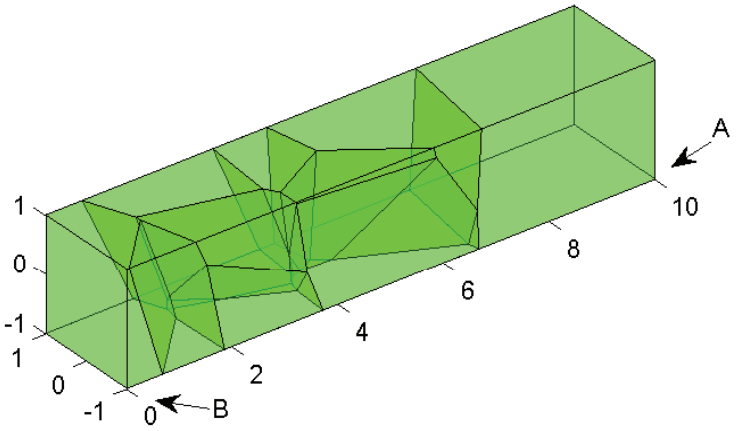

Figure 5: Mesh configuration used for overall test of performances of different VCFEMs

6 T-Trefftz VCFEMs with Spherical Inclusions/Voids

6.1 T-Trefftz Trial Displacement Fields for Different Types of Inhomogeneities

Consider a linear elastic solid undergoing infinitesimal elasto-static deformation. The governing equation can be written in terms of displacements, which is the

Table 5: Computed and exact solution of cantilever beam in Fig. 5 under end shear or bending moment

Element Type	End Bending	
	v_A	σ_B
VCFEM-TT-BVP	71.2	2962.9
VCFEM-TT-C	72.5	3009.1
Exact	100.3	3000.0

Navier's equation:

$$(\lambda+\mu)\theta_{,i}+\mu\Delta u_i=0 \tag{49}$$

The boundary conditions are:

$$u_i=\overline{u}_i \text{ at } S_u \tag{50}$$

$$n_j\sigma_{ij}=\bar{t}_i \text{ at } S_t \tag{51}$$

We consider that the domain Ω is discretized into elements Ω^e with element boundary $\partial\Omega^e$, each element boundary can be divided into S_u^e, S_t^e, ρ^e, which are intersections of $\partial\Omega^e$ with S_u, S_t and other element boundaries respectively. For elements developed in this study, an inclusion or void Ω_c^e is present inside each element, which satisfy $\Omega_c^e \subset \Omega^e, \partial\Omega_c^e \cap \partial\Omega^e = \emptyset$, see Fig. 6. We denote the matrix material in each element as Ω_m^e, such that $\Omega_m^e = \Omega^e - \Omega_c^e$.

When an elastic inclusion is considered, we denote the displacement field in Ω_m^e and Ω_c^eas u_i^m and u_i^c, the strain and stress fields corresponding to which are $\varepsilon_{ij}^m, \sigma_{ij}^m$ and $\varepsilon_{ij}^c, \sigma_{ij}^c$ respectively. We also denote the displacement field along $\partial\Omega^e$as $\tilde{u}_i^m$, which is inter-element compatible, by using Barycentric coordinates as nodal shape functions. Then, in addition tou_i^c satisfying(49)ineach Ω_c^e, u_i^m satisfying(49)ineach Ω_m^e, satisfying(51) at S_t^e, $\tilde{u}_i^m$ satisfying(50) at S_u^e,displacement continuity and traction reciprocity conditions at each ρ^eshould be considered:

$$u_i^m=\tilde{u}_i^m \text{ at } \partial\Omega^e \tag{52}$$

$$\left(n_j\sigma_{ij}^m\right)^+ + \left(n_j\sigma_{ij}^m\right)^- = 0 \text{ at } \rho^e \tag{53}$$

Displacement continuity and traction reciprocity conditions at $\partial\Omega_c^e$ should also be considered:

$$u_i^m=u_i^c \text{ at } \partial\Omega_c^e \tag{54}$$

$$-n_j\sigma_{ij}^m+n_j\sigma_{ij}^c=0 \text{ at } \partial\Omega_c^e \tag{55}$$

where n_j is the unit outer-normal vector at $\partial\Omega_c^e$.

When a rigid inclusion is considered, because only rigid-body displacement is allowed for the inclusion, there is no need to assume u_i^c. The following conditions need to be satisfied at $\partial\Omega_c^e$:

$$u_i^m(\text{non-rigid-body}) = 0 \text{ at } \partial\Omega_c^e \tag{56}$$

$$\begin{aligned} &\int_{\partial\Omega_c^e} n_j \sigma_{ij}^m dS = 0 \\ &\int_{\partial\Omega_c^e} e_{ghi} x_h n_j \sigma_{ij}^m dS = 0 \end{aligned} \tag{57}$$

When a void is to be considered, for VCFEM-TT-BVP,$\tilde{u}_i^c$ is assumed only along $\partial\Omega_c^e$. The following displacement continuity and traction free conditions are to be satisfied:

$$u_i^m = \tilde{u}_i^c \text{ at } \partial\Omega_c^e \tag{58}$$

$$n_j \sigma_{ij}^m = 0 \text{ at } \partial\Omega_c^e \tag{59}$$

For VCFEM-TT-C, on the other hand, there is no need to assume such a boundary field $\tilde{u}_i^c$. Only (59) needs to be satisfied at $\partial\Omega_c^e$.

It should be noted that, for a priori equilibrated displacement fields, condition (57) is a necessary condition of (55)or (59). Hence, for problems with elastic inclusion or voids, condition (57) is satisfied as long as conditions (55) or (59) are satisfied.

In T-Trefftz elements derived in this study, u_i^m, u_i^c satisfy (49) as well as (57)a priori, and all other conditions as shown in (50)-(59) are satisfied using variational principles or using collocation method. Such displacement fields can be expressed in terms of Papkovich-Neuber potentials. When a spherical inclusion or void is present, as shown in Fig. 6, the source point is put in the center of the sphere and we use two types of spherical harmonics as Papkovich-Neuber potentials:

$$\begin{aligned} \mathbf{B}_{mp} &= \sum_{n=0}^{M} \left(\frac{R}{R_{mp}}\right)^n \left\{ \mathbf{a}_0^0 YC_0^0(\theta,\phi) + \sum_{l=1}^{n} \left[\mathbf{a}_n^l YC_n^l(\theta,\phi) + \mathbf{b}_n^l YS_n^l(\theta,\phi) \right] \right\} \\ \mathbf{B}_{mk} &= \sum_{n=0}^{N} \left(\frac{R}{R_{mk}}\right)^{-(n+1)} \left\{ \mathbf{c}_0^0 YC_0^0(\theta,\phi) + \sum_{l=1}^{n} \left[\mathbf{d}_n^l YC_n^l(\theta,\phi) + \mathbf{d}_n^l YS_n^l(\theta,\phi) \right] \right\} \end{aligned} \tag{60}$$

$\mathbf{B}_{mp}$ are spherical harmonics for the internal problems, whichare non-singular in the whole domain. And $\mathbf{B}_{mk}$ are spherical harmonics for the external problems, which are singular at the source point:

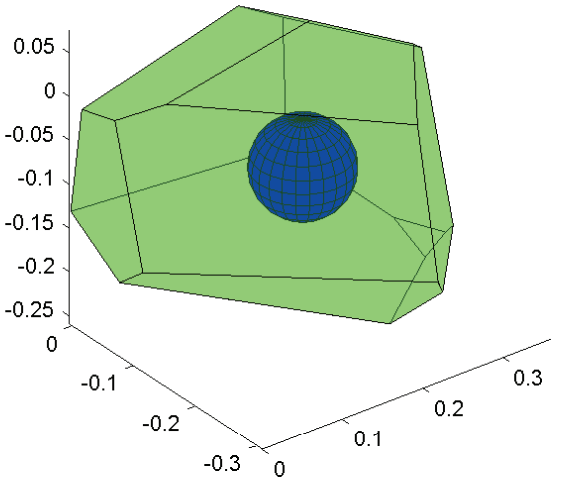

Figure 6: A 3D VCFEM with a spherical inclusion/void

Two characteristic lengths R_{mk} and R_{mp} are defined. R_{mk} is equal to the minimum distance between the source point S^e and any point in Ω_m^e, therefore $\left(\frac{R}{R_{mk}}\right)^{-(n+1)}$ is confined between 0 and 1 for any positive n. For a spherical inclusion/void, it is obvious that R_{mk} is equal to the radius of the sphere.

R_{mp} is equal to the maximum distance between the source point S^e and any point in Ω_m^e, therefore $\left(\frac{R}{R_{mk}}\right)^{n}$ is confined between 0 and 1 for any positive n.

And the displacement field in the matrix is express as:

$$\begin{aligned}
&\mathbf{u}_m = \mathbf{u}_{mp} + \mathbf{u}_{mk} \\
&\mathbf{u}_{mp} = \left[4(1-\nu_m)\mathbf{B}_{mp} + \mathbf{R}\cdot\nabla\mathbf{B}_{mp} - \mathbf{R}\nabla\cdot\mathbf{B}_{mp})\right]/2G_m \\
&\mathbf{u}_{mk} = \left[4(1-\nu_m)\mathbf{B}_{mk} - \nabla\mathbf{R}_{mk}\cdot\mathbf{B}\right]/2G_m
\end{aligned} \tag{61}$$

When a spherical elastic inclusion is considered, u_i^c can be express using the spherical harmonics for internal problems:

$$\begin{aligned}
&\mathbf{u}_c = \mathbf{u}_{cp} = \left[4(1-\nu_c)\mathbf{B}_{cp} + \mathbf{R}\cdot\nabla\mathbf{B}_{cp} - \mathbf{R}\nabla\cdot\mathbf{B}_{cp})\right]/2G_c \\
&\mathbf{B}_{cp} = \sum_{n=0}^{L}\left(\frac{R}{R_{cp}}\right)^n\left\{\mathbf{e}_0^0 Y C_0^0(\theta,\phi) + \sum_{l=1}^{n}\left[\mathbf{e}_n^l Y C_n^l(\theta,\phi) + \mathbf{f}_n^l Y S_n^l(\theta,\phi)\right]\right\}
\end{aligned} \tag{62}$$

R_{cp} is equal to the maximum distance between the source point S^e and any point in Ω_c^e, therefore $\left(\frac{R}{R_{cp}}\right)^n$ is confined between 0 and 1 for any positive n.

When a rigid inclusion is considered, u_i^cdoes not need to be assumed. Assuming u_i^m is good enough in order to develop finite element equations.

When a void is considered, for VCFEM-TT-BVP, $\tilde{u}_i^c$ is assumed only at $\partial\Omega_c$. We assume

$$\begin{aligned}
&\tilde{\mathbf{u}}_c = \tilde{\mathbf{u}}_{cp} = \left[4(1-\nu_m)\tilde{\mathbf{B}}_{cp} + \mathbf{R}\cdot\nabla\tilde{\mathbf{B}}_{cp} - \mathbf{R}\nabla\cdot\tilde{\mathbf{B}}_{cp})\right]/2G_m \\
&\tilde{\mathbf{B}}_{cp} = \sum_{n=0}^{L}\left(\frac{R}{R_{cp}}\right)^n\left\{\mathbf{g}_0^0 YC_0^0(\theta,\phi) + \sum_{l=1}^{n}\left[\mathbf{g}_n^l YC_n^l(\theta,\phi) + \mathbf{h}_n^l YS_n^l(\theta,\phi)\right]\right\}
\end{aligned} \tag{63}$$

Now that the displacement fields are defined, the undetermined parameters can be related to nodal displacements of the element using either multi-field boundary variational principles or using the collocation method, which is similar to the approaches as shown in section 5, for VCFEM-TTs without inclusions/voids.

It should be noted that, the six rigid-body modes should be eliminated beforehand for VCFEM-TT-BVP, but should be preserved for VCFEM-TT-C. All other modes are independent, non-rigid-body modes.

It also should be noted that the following three modes correspond to concentrated forces at the source point (Kelvin's solutions). They are the only three modes that contribute to the total resultant forces on $\partial\Omega_c$:

$$\begin{aligned}
&\mathbf{c}_0^0 = \begin{Bmatrix}1 & 0 & 0\end{Bmatrix}^T \\
&\mathbf{c}_0^0 = \begin{Bmatrix}0 & 1 & 0\end{Bmatrix}^T \\
&\mathbf{c}_0^0 = \begin{Bmatrix}0 & 0 & 1\end{Bmatrix}^T
\end{aligned} \tag{64}$$

And the following three modes correspond to concentrated moments at the source point. They are the only three modescontribute to the total resultant moments on $\partial\Omega_c$:

$$\begin{aligned}
&\mathbf{c}_1^0 = \begin{Bmatrix}1 & 0 & 0\end{Bmatrix}^T, \quad \mathbf{c}_1^1 = \begin{Bmatrix}0 & 0 & \sqrt{2}\end{Bmatrix}^T \\
&\mathbf{c}_1^0 = \begin{Bmatrix}0 & 1 & 0\end{Bmatrix}^T, \quad \mathbf{c}_1^1 = \begin{Bmatrix}0 & \sqrt{2} & 0\end{Bmatrix}^T \\
&\mathbf{c}_1^1 = \begin{Bmatrix}0 & 1 & 0\end{Bmatrix}^T, \quad \mathbf{d}_1^1 = \begin{Bmatrix}-1 & 0 & 0\end{Bmatrix}^T
\end{aligned} \tag{65}$$

Moreover, the displacement assumptions considered in this section are all invariant with respect to change of coordinate systems. Therefore, the element stiffness matrices developed from these displacement assumptions are expected to be invariant.

6.2 T-Trefftz VCFEMs Using Multi-Field Boundary Variational Principles

In this section, T-Trefftz VCFEMs are developed using multi-field boundary variational principles.

An inter-element compatible displacement field $\tilde{u}_i^m$ is assumed at $\partial\Omega^e$ with Wachspress coordinates as nodal shape functions. Using matrix and vector notation, we have:

$$\tilde{\mathbf{u}}_m = \tilde{\mathbf{N}}_m \mathbf{q} \text{ at } \partial\Omega^e \tag{66}$$

The displacement field in Ω_m^e and its corresponding traction field t_i^m at $\partial\Omega_m^e, \partial\Omega_c^e$ as:

$$\begin{aligned} &\mathbf{u}_m = \mathbf{N}_m \boldsymbol{\alpha} \text{ in } \Omega_m^e \\ &\mathbf{t}_m = \mathbf{R}_m \boldsymbol{\alpha} \text{ at } \partial\Omega_m^e, \partial\Omega_c^e \end{aligned} \tag{67}$$

When an elastic inclusion is to be considered, the displacement field in the inclusion is independently assumed. We have:

$$\begin{aligned} &\mathbf{u}_c = \mathbf{N}_c \boldsymbol{\beta} \text{ in } \Omega_c^e \\ &\mathbf{t}_c = \mathbf{R}_c \boldsymbol{\beta} \text{ at } \partial\Omega_c^e \end{aligned} \tag{68}$$

Therefore, finite element equations can be derived using the following three-field boundary variational principle:

$$\begin{aligned} \pi_3(\tilde{u}_i^m, u_i^m, u_i^c) = &\sum_e \left\{ -\int_{\partial\Omega^e + \partial\Omega_c^e} \frac{1}{2} t_i^m u_i^m dS + \int_{\partial\Omega_m^e} t_i^m \tilde{u}_i^m dS - \int_{S_t^e} \bar{t}_i \tilde{u}_i^m dS \right\} \\ &+ \sum_e \left\{ \int_{\partial\Omega_c^e} t_i^m u_i^c dS + \int_{\partial\Omega_c^e} \frac{1}{2} t_i^c u_i^c dS \right\} \end{aligned} \tag{69}$$

This leads to finite element equations:

$$\delta \begin{Bmatrix} \mathbf{q} \\ \boldsymbol{\beta} \end{Bmatrix}^T \begin{bmatrix} \mathbf{G}_{\alpha q}^T \mathbf{H}_{\alpha\alpha}^{-1} \mathbf{G}_{\alpha q} & \mathbf{G}_{\alpha q}^T \mathbf{H}_{\alpha\alpha}^{-1} \mathbf{G}_{\alpha\beta} \\ \mathbf{G}_{\alpha\beta}^T \mathbf{H}_{\alpha\alpha}^{-1} \mathbf{G}_{\alpha q} & \mathbf{G}_{\alpha\beta}^T \mathbf{H}_{\alpha\alpha}^{-1} \mathbf{G}_{\alpha\beta} + \mathbf{H}_{\beta\beta} \end{bmatrix} \begin{Bmatrix} \mathbf{q} \\ \boldsymbol{\beta} \end{Bmatrix} = \delta \begin{Bmatrix} \mathbf{q} \\ \boldsymbol{\beta} \end{Bmatrix}^T \begin{Bmatrix} \mathbf{Q} \\ \mathbf{0} \end{Bmatrix} \tag{70}$$

where

$$\begin{aligned} \mathbf{G}_{\alpha q} &= \int_{\partial\Omega^e} \mathbf{R}_m^T \tilde{\mathbf{N}}_m dS \\ \mathbf{H}_{\alpha\alpha} &= \int_{\partial\Omega^e + \partial\Omega_c^e} \mathbf{R}_m^T \mathbf{N}_m dS \\ \mathbf{H}_{\beta\beta} &= \int_{\partial\Omega_c^e} \mathbf{R}_c^T \mathbf{N}_c dS \\ \mathbf{Q} &= \int_{S_t^e} \tilde{\mathbf{N}}_m^T \bar{\mathbf{t}} dS \end{aligned} \tag{71}$$

This equation can be further simplified by static-condensation.

When the inclusion is rigid, u_i^c does not need to be assumed, and we use the following variational principle:

$$\pi_4(\tilde{u}_i^m, u_i^m) = \sum_e \left\{ -\int_{\partial\Omega^e + \partial\Omega_c^e} \frac{1}{2} t_i^m u_i^m dS + \int_{\partial\Omega_m^e} t_i^m \tilde{u}_i^m dS - \int_{S_t^e} \bar{t}_i \tilde{u}_i^m dS \right\} \tag{72}$$

The corresponding finite element equations are:

$$\sum_e \left(\delta\mathbf{q}^T \mathbf{G}_{\alpha q}^T \mathbf{H}_{\alpha\alpha}^{-1} \mathbf{G}_{\alpha q} \mathbf{q} - \delta\mathbf{q}^T \mathbf{Q} \right) = 0 \tag{73}$$

When the element includes a void instead of an elastic/rigid inclusion, $\tilde{u}_i^c$ is merely assumed at $\partial\Omega_c^e$. We have:

$$\tilde{\mathbf{u}}_c = \tilde{\mathbf{N}}_c \boldsymbol{\gamma} \text{ at } \partial\Omega_c^e \tag{74}$$

We use the following variational principle:

$$\begin{aligned} \pi_5(\tilde{u}_i^m, u_i^m, \tilde{u}_i^c) = &\sum_e \left\{ -\int_{\partial\Omega^e + \partial\Omega_c^e} \frac{1}{2} t_i^m u_i^m dS + \int_{\partial\Omega_m^e} t_i^m \tilde{u}_i^m dS - \int_{S_t^e} \bar{t}_i \tilde{u}_i^m dS \right\} \\ &+ \sum_e \int_{\partial\Omega_c^e} t_i^m \tilde{u}_i^c dS \end{aligned} \tag{75}$$

The corresponding finite element equations are:

$$\delta \begin{Bmatrix} \mathbf{q} \\ \boldsymbol{\gamma} \end{Bmatrix}^T \begin{bmatrix} \mathbf{G}_{\alpha q}^T \mathbf{H}_{\alpha\alpha}^{-1} \mathbf{G}_{\alpha q} & \mathbf{G}_{\alpha q}^T \mathbf{H}_{\alpha\alpha}^{-1} \mathbf{G}_{\alpha\gamma} \\ \mathbf{G}_{\alpha\gamma}^T \mathbf{H}_{\alpha\alpha}^{-1} \mathbf{G}_{\alpha q} & \mathbf{G}_{\alpha\gamma}^T \mathbf{H}_{\alpha\alpha}^{-1} \mathbf{G}_{\alpha\gamma} \end{bmatrix} \begin{Bmatrix} \mathbf{q} \\ \boldsymbol{\gamma} \end{Bmatrix} = \delta \begin{Bmatrix} \mathbf{q} \\ \boldsymbol{\gamma} \end{Bmatrix}^T \begin{Bmatrix} \mathbf{Q} \\ \mathbf{0} \end{Bmatrix} \tag{76}$$

where

$$\mathbf{G}_{\alpha\gamma} = \int_{\partial\Omega_c^e} \mathbf{R}_m^T \tilde{\mathbf{N}}_c dS \tag{77}$$

Similarly, this equation can be further simplified by static-condensation.

It should be pointed out that VCFEM-TT-BVPs developed in this section, with spherical voids/inclusions, are plagued by LBB conditions, because Lagrange multipliers are involved. VCFEM-TT-Cs without involving LBB conditions are developed in section 6.3, by using collocation method to enforcing the compatibility between independently assumed fields.

6.3 T-Trefftz VCFEMs Using Collocation and a Primitive Field Boundary Variational Principle

In this section, we develop 3D VCFEM-TTs using collocation method and a primitive field variational principle, in a similar fashion to its 2D versions as shown in [Dong and Atluri (2012a)].

A finite number of collocation points are selected along $\partial\Omega^e$ and $\partial\Omega_c^e$, denoted as $x_i^{mp} \in \partial\Omega^e, p = 1,2....$, and $x_i^{cq} \in \partial\Omega_c^e, q = 1,2....$

Collocations are carried out in the following manner:

1. When an elastic inclusion is considered, we enforce the following conditions at corresponding collocation points:

$$\begin{aligned} &u_i^m(x_j^{mp},\boldsymbol{\alpha}) = \tilde{u}_i(x_j^{mp},\mathbf{q}) \quad x_j^{mp} \in \partial\Omega^e \\ &u_i^m(x_j^{cq},\boldsymbol{\alpha}) - u_i^c(x_j^{cq},\boldsymbol{\beta}) = 0 \quad x_j^{cq} \in \partial\Omega_c^e \\ &wt_i^m(x_j^{cq},\boldsymbol{\alpha}) + wt_i^c(x_j^{cq},\boldsymbol{\beta}) = 0 \quad x_j^{cq} \in \partial\Omega_c^e \end{aligned} \tag{78}$$

$\boldsymbol{\alpha},\boldsymbol{\beta}$ are related to $\mathbf{q}$ in the following way:

$$\begin{aligned} \boldsymbol{\alpha} &= \mathbf{C}_{\alpha q}^1 \mathbf{q} \\ \boldsymbol{\beta} &= \mathbf{C}_{\beta q}^1 \mathbf{q} \end{aligned} \tag{79}$$

2. When the inclusion is rigid, there is no need to assume u_i^c, and the following collocations are considered:

$$\begin{aligned} &u_i^m(x_j^{mp},\boldsymbol{\alpha}) = \tilde{u}_i(x_j^{mp},\mathbf{q}) \quad x_j^{mp} \in \partial\Omega^e \\ &u_i^m(\text{non-rigid-body},x_j^{cq},\boldsymbol{\alpha}) = 0 \quad x_j^{cq} \in \partial\Omega_c^e \end{aligned} \tag{80}$$

We obtain:

$$\alpha = \mathbf{C}_{\alpha q}^2 \mathbf{q} \tag{81}$$

3. When a void is considered instead of a inclusion, there is no need to assume u_i^cor $\tilde{u}_i^c$. The following conditions are enforced:

$$\begin{aligned} &u_i^m(x_j^{mp},\boldsymbol{\alpha}) = \tilde{u}_i(x_j^{mp},\mathbf{q}) \quad x_j^{mp} \in \partial\Omega^e \\ &wt_i^m(x_j^{cq},\boldsymbol{\alpha}) = 0 \quad x_j^{cq} \in \partial\Omega_c^e \end{aligned} \tag{82}$$

By solving(82), we have:

$$\boldsymbol{\alpha} = \mathbf{C}_{\alpha q}^3 \mathbf{q} \tag{83}$$

It should be noted that, in (78)and (82), a parameter w is used to weigh the collocation equations for tractions, so that they have the same order of importance as collocation equations for displacements. For displacement fields assumed in section 6.1, it is obvious that a proper choice of w is $w = R_{mk}/2G_m$. It should also be pointed out that, for the over-determined system of equations obtained using either (78), (80), or (82), the least square solution as discussed in (44) is obtained.

Now that the interior displacement field is related to nodal displacements, finite element equations can be derived from the following primitive-field boundary variational principle, as used in section 5 for elements without inclusions/voids:

$$\pi_2(u_i) = \sum_e \left\{ \int_{\partial\Omega^e} \frac{1}{2} t_i u_i dS - \int_{S_t^e} \bar{t}_i u_i dS \right\} \tag{84}$$

Substituting corresponding displacement fields into (84), we obtain finite element equations:

$$\begin{aligned} &\sum_m \left(\delta\mathbf{q}^T {\mathbf{C}^s_{\alpha q}}^T \mathbf{M}_{\alpha\alpha} \mathbf{C}^s_{\alpha q} \mathbf{q} - \delta\mathbf{q}^T \mathbf{Q} \right) = 0, \ s = 1, 2 \text{ or } 3 \\ &\mathbf{M}_{\alpha\alpha} = \int_{\partial\Omega^e} \mathbf{R}_m^T \mathbf{N}_m dS \end{aligned} \tag{85}$$

When s is equal to 1, 2, and 3, ${\mathbf{C}^s_{\alpha q}}^T \mathbf{M}_{\alpha\alpha} \mathbf{C}^s_{\alpha q}$ is the stiffness matrix for VCFEM-TTs with an elastic inclusion, a rigid inclusion, and a void respectively.

Because in the development of VCFEM-TT-C, integration of only one matrix $\mathbf{M}_{\alpha\alpha}$ along the outer boundary is needed, and collocatoin along the inner boundary require less points where the basis functions are evaluated, VCFEM-TT-C is expected to be computationally more efficient than VCFEM-TT-BVP. Also, as explained previously, VCFEM-TT-C does not suffer from LBB conditions, which is a tremendous advantage of VCFEM-TT-C over VCFEM-TT-BVP.

6.4 Numerical Examples

Firstly, we illustrate the reason why we use characteristic lengths to scale the T-Trefftz trial functions. See Fig. 7 for the geometry of the element. Material properties of the matrix are $E_m = 1, v_m = 0.25$. Three kinds of heterogeneities are considered: an elastic inclusion with $E_c = 2, v_c = 0.3$, a rigid inclusion, and a void. Stiffness matrices of VCFEM-TT-C are computed, with and without using characteristic lengths to scale T-Trefftz trial functions. Condition numbers of the coefficient matrix of equationsare shown in Tab. 5. We can clearly see that by scaling the T-Trefftz functions using characteristic lengths, the resulting systems of equations have significantly smaller condition number. Although not shown here,

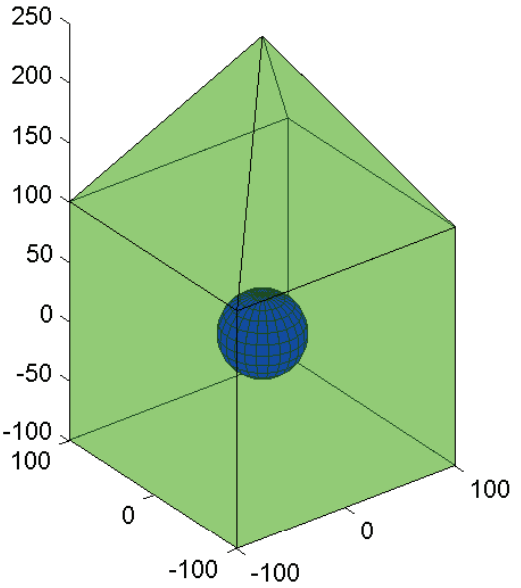

Figure 7: An element with a spherical inclusion/void used for condition number test, eigenvalue test, and patch test

Table 6: Condition number of coefficient matrices of equations used to relate $\boldsymbol{\alpha}, \boldsymbol{\beta}$ to $\mathbf{q}$ using the collocation method with/without using characteristic lengths to scale T-Trefftz Trial functions for the element shown in Fig. 7

	Elastic Inclusion		Rigid Inclusion		Void	
Characteristic Length	Scaled	Not scaled	Scaled	Not scaled	Scaled	Not scaled
Condition number	1.08×10^{3}	3.7×10^{35}	2.8×10^{34}	2.3×10^{33}	2.8×10^{3}	2.6×10^{35}

scaling T-Trefftz trial functions using characteristic lengths also has similar effect on VCFEM-TT-BVP.

We also compare the CPU time required for computing the stiffness matrix of the element shown in Fig. 7, using different VCFEM-TTs. The CPU time required is shown in Tab. 7. As can be seen, VCFEM-TT-C needsless time for computing one element than that for VCFEM-TT-BVP. The computational time for either of

these two types of VCFEM-TTs should be much less than VCFEMs developed in [Ghosh and Moorthy (2004)].

Table 7: CPU time required for computing the stiffness matrix of the element in Fig. 7

CPU Time (seconds)	VCFEM-TT-BVP	VCFEM-TT-C
	2.42	1.51

Using the same element, we compute the eigenvalues of element stiffness matrices of different VCFEMs. This is conducted in the original and rotated global Cartesian coordinate system. Experimental results are shown in Tab. 8-10

As can clearly be seen, these elements are stable and invariant for this element, because additional zero energy modes do not exist, and eigenvalues do not vary with respect to change of coordinate systems. However, this does not mean that LBB conditions are satisfied by VCFEM-TT-BVP for an arbitrary element.

We also conduct the one-element patch test. The same element is considered. The materials of the matrix and the inclusion are the same, with material properties $E = 1, v = 0.25$. A uniform traction is applied to the upper faces. The displacements in the lower face are prescribed to be the exact solution. Experimental results are shown in Tab. 11.

As can be seen, VCFEM-TT-BVP can pass the patch test with errors equal to or less than an order of 10^{-8}. Although the error for VCFEM-TT-C is larger, but still in an order of 10^{-3}. We consider the performance of all VCFEMs to be satisfactory in this one-element patch test.

In order to evaluate the overall performances of different VCFEMs for modeling problems with inclusions or voids, we consider the following problem: an infinite medium with a spherical elastic/rigid inclusion or void in it. Exact solution of all of these three problems: an elastic inclusion, a rigid inclusion, or a void, can be solved using Eshelby's solution and the equivalent inclusion method. For details of the exact solution, see [Eshelby (1957); Nemat-Nasser and Hori (1999)].

The material properties of the matrix are $E_m = 1, v_m = 0.25$. When an elastic inclusion is considered, the material properties of the inclusion are $E_c = 2, v_c = 0.3$. The magnitude of the remote tension P in the direction of x_3 is equal to 1. The radius of the inclusion/void is 0.1. For numerical implementation, the infinite medium is truncated to a finite cube. The length of each side of the truncated cube is equal to2. For all three cases with an elastic/rigid inclusion or a void, only one element is used. Traction boundary conditions are applied to the outer-boundary of the element. Least number of nodal displacements are prescribed to the exact solution.

Table 8: Eigenvalues of stiffness matrices of different VCFEMs when an elastic inclusion is considered

Eigenvalues Rotation=0˚&45˚	VCFEM-TT-BVP	VCFEM-TT-C
1	2.3383	2.3455
2	1.0878	1.1022
3	1.0805	1.0909
4	0.8408	0.8434
5	0.8408	0.8434
6	0.8349	0.7703
7	0.6267	0.6164
8	0.6161	0.6048
9	0.6002	0.6015
10	0.6002	0.6015
11	0.5530	0.5373
12	0.5408	0.5296
13	0.5408	0.5296
14	0.5029	0.5040
15	0.2984	0.2965
16	0.2511	0.2546
17	0.2511	0.2546
18	0.1915	0.1834
19	0.1915	0.1834
20	0.1692	0.1737
21	0.1219	0.1323
22	0.0000	0.0000
23	0.0000	0.0000
24	0.0000	0.0000
25	0.0000	0.0000
26	0.0000	0.0000
27	0.0000	0.0000

We compare the computed σ_{11} along axis x_3, σ_{33} along axis x_1, to that of the exact solution. As shown in Fig. 9-11, no matter an elastic inclusion, a rigid inclusion, or a void is considered, VCFEM-TTs always give very accurate computed stresses, even though only one element is used. For this reason, we consider VCFEM-TTs very efficient for micromechanical modeling of heterogeneous materials.

We also use the VCFEM-TTs developed in this study to study the stiffness of het-

Table 9: Eigenvalues of stiffness matrices of different VCFEMs when a rigid inclusion is considered

Eigenvalues Rotation=0˚&45˚	VCFEM-TT-BVP	VCFEM-TT-C
1	2.4003	2.4081
2	1.1161	1.1280
3	1.1098	1.1187
4	0.8657	0.8686
5	0.8657	0.8686
6	0.8453	0.7826
7	0.6421	0.6205
8	0.6205	0.6115
9	0.6074	0.6099
10	0.6074	0.6099
11	0.5553	0.5406
12	0.5431	0.5302
13	0.5431	0.5302
14	0.5077	0.5078
15	0.3018	0.3005
16	0.2531	0.2557
17	0.2531	0.2557
18	0.1919	0.1836
19	0.1919	0.1836
20	0.1699	0.1744
21	0.1227	0.1330
22	0.0000	0.0000
23	0.0000	0.0000
24	0.0000	0.0000
25	0.0000	0.0000
26	0.0000	0.0000
27	0.0000	0.0000

erogeneous materials. A Unit Cell model of Al/SiC material is considered. The material properties are: $E_{\mathrm{Al}} = 74GPa, \nu_{\mathrm{Al}} = 0.33, E_{SiC} = 410GPa, \nu_{SiC} = 0.19$. The volume fraction of SiC is 20%. This model was studied in [Chawla, Ganesh, Wunsch (2004)], using around 76,000 ten-node tetrahedral elements with ABAQUS. However, in this study, we use just one VCFEM, see in Fig. 12. As shown in Tab. 12, although only one element is used, the homogenized Young's modulus is quite close to what is obtained by using round 76,000 ten-node tetrahedral elements with

Table 10: Eigenvalues of stiffness matrices of different VCFEMs when a void is considered

Eigenvalues Rotation=0˚&45˚	VCFEM-TT-BVP	VCFEM-TT-C
1	2.2681	2.2617
2	1.0640	1.0656
3	1.0564	1.0546
4	0.8632	0.8510
5	0.8241	0.8236
6	0.8241	0.8236
7	0.6278	0.6340
8	0.6113	0.6134
9	0.5963	0.5867
10	0.5963	0.5867
11	0.5707	0.5542
12	0.5707	0.5542
13	0.5602	0.5479
14	0.5029	0.5086
15	0.2994	0.2977
16	0.2518	0.2609
17	0.2518	0.2609
18	0.1978	0.1862
19	0.1978	0.1862
20	0.1726	0.1828
21	0.1257	0.1226
22	0.0000	0.0000
23	0.0000	0.0000
24	0.0000	0.0000
25	0.0000	0.0000
26	0.0000	0.0000
27	0.0000	0.0000

Table 11: Performances of different VCFEMs in patch test

Error	VCFEM-TT-BVP	VCFEM-TT-C
	1.0×10^{-8}	6.5×10^{-3}

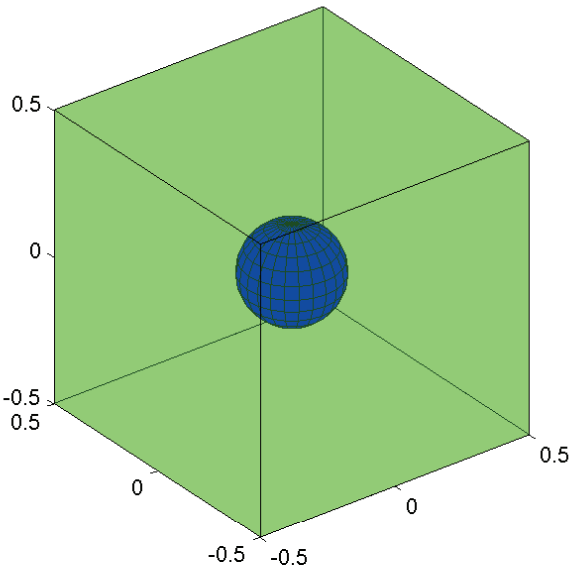

Figure 8: A spherical elastic/rigid inclusion or hole under remote tension

ABAQUS.

Table 12: Homogenized Young's modulus using different methods

Method	Young's Modulus (GPa)
VCFEM-TT-BVP	103.8
VCFEM-TT-C	98.8
ABAQUS	100.0

We also study a RVE of Al/SiC material, with 125 randomly distributed spherical SiC particles. The RVE is shown in Fig. 13, discretized with 125 VCFEMs developed in this study. The material properties of Al and SiC are taken the same as those in the last example. The size of the RVE is 100 μm $\times$ 100 μm $\times$ 100 μm.

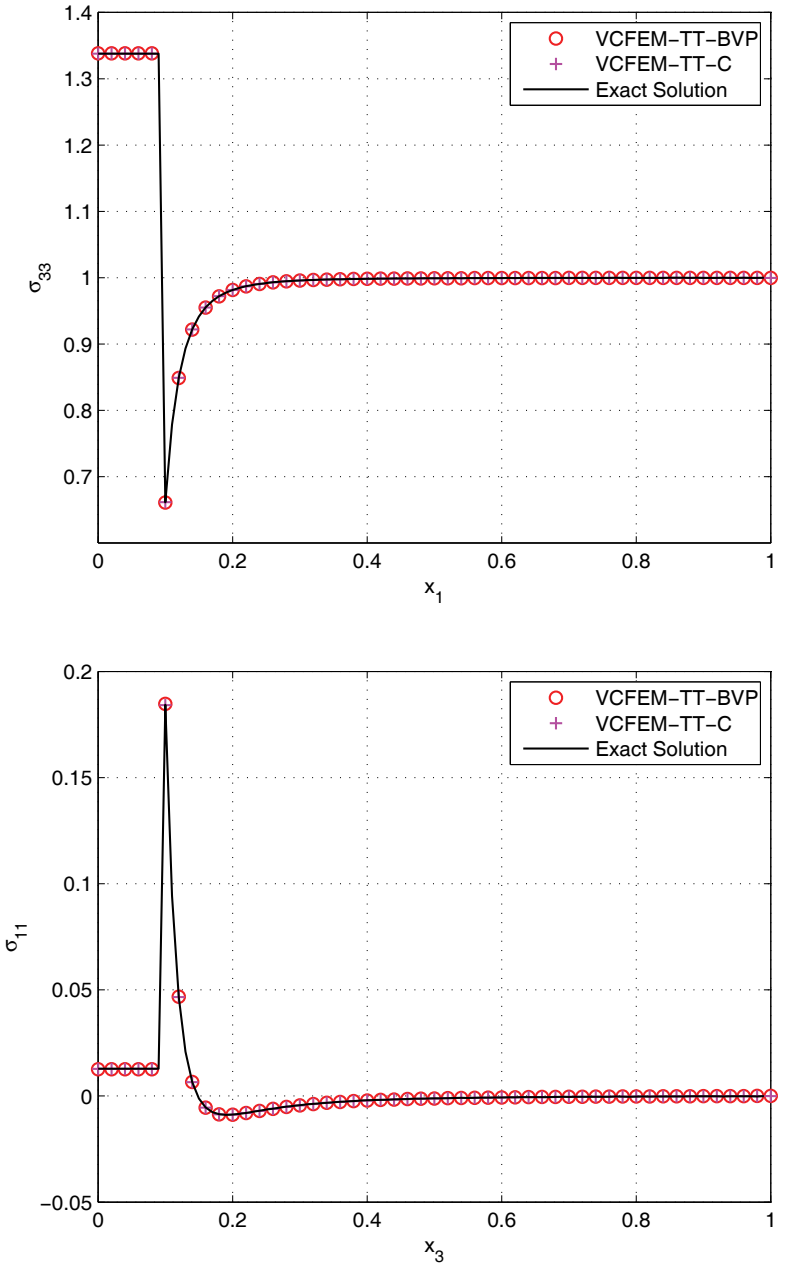

Figure 9: Computed σ_{11} along axis x_3, σ_{33} along axis x_1 for the problem with an elastic inclusion

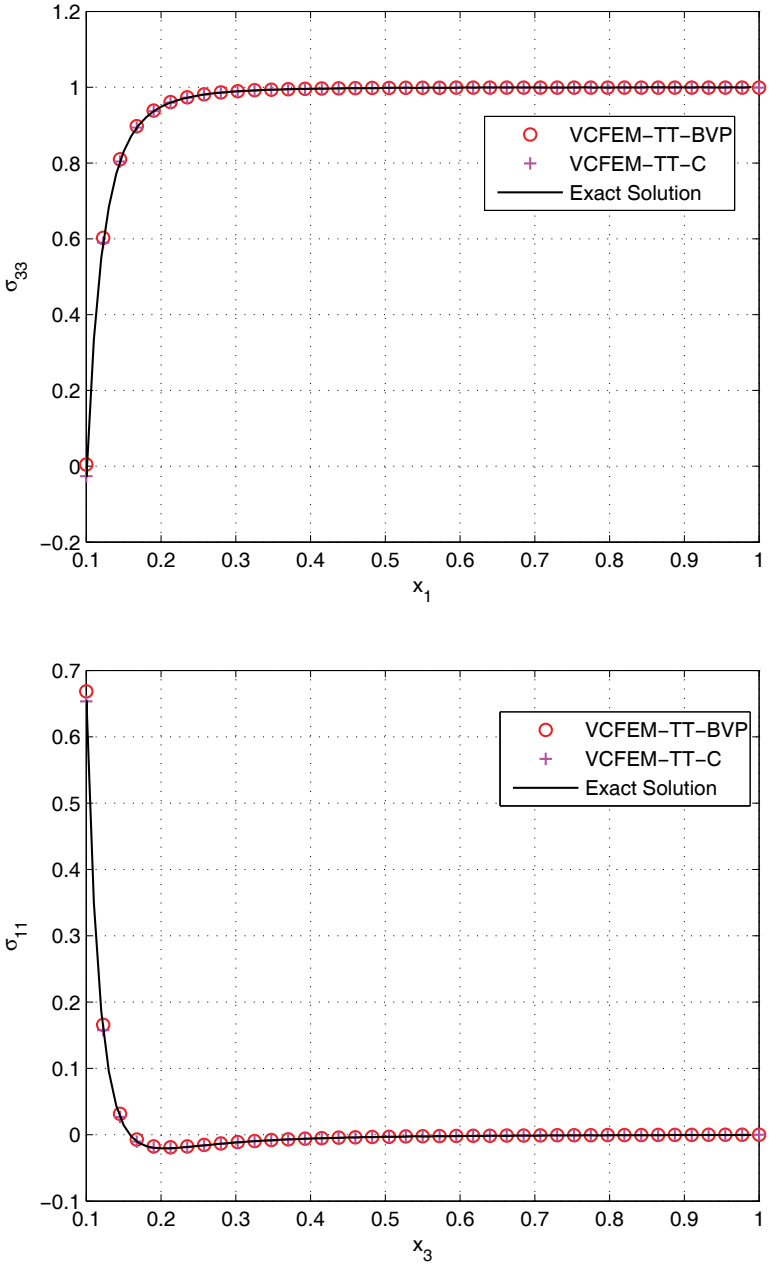

Figure 10: Computed σ_{11} along axis x_3, σ_{33} along axis x_1 for the problem with a rigid inclusion

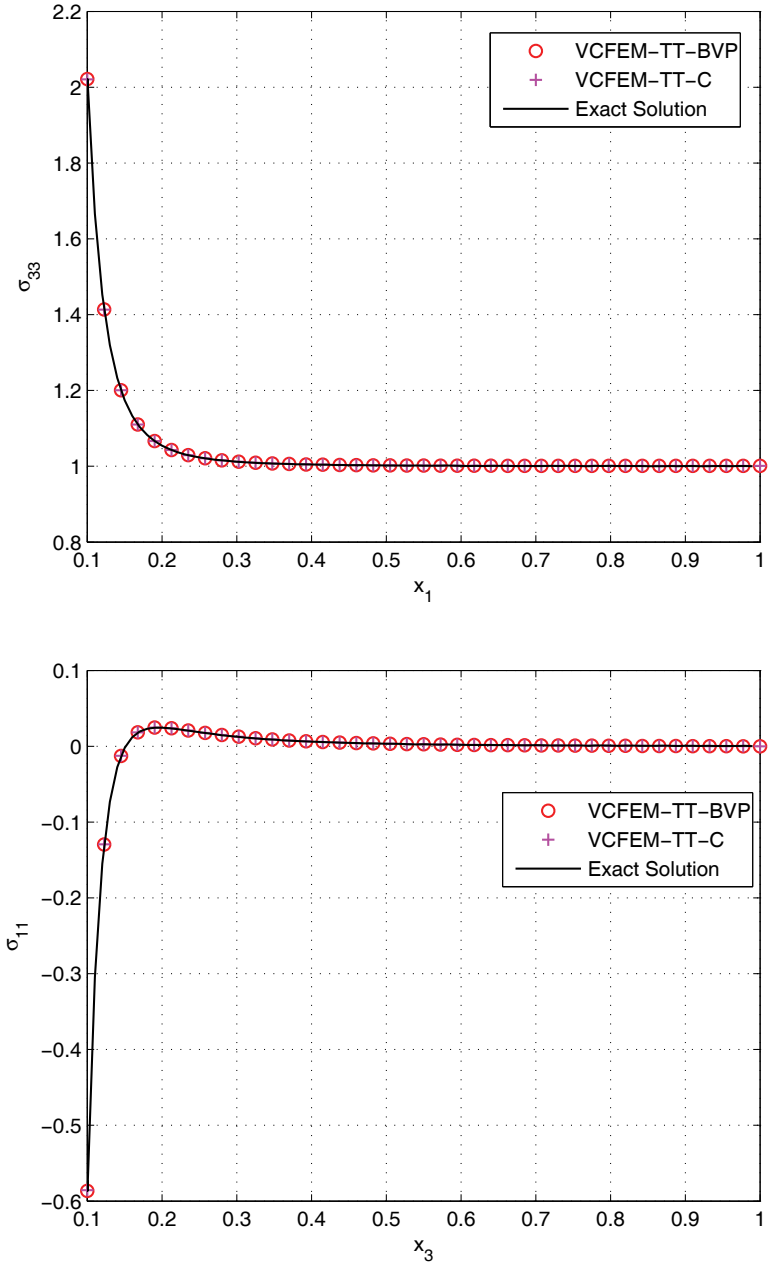

Figure 11: Computed σ_{11} along axis x_3, σ_{33} along axis x_1 for the problem with a void

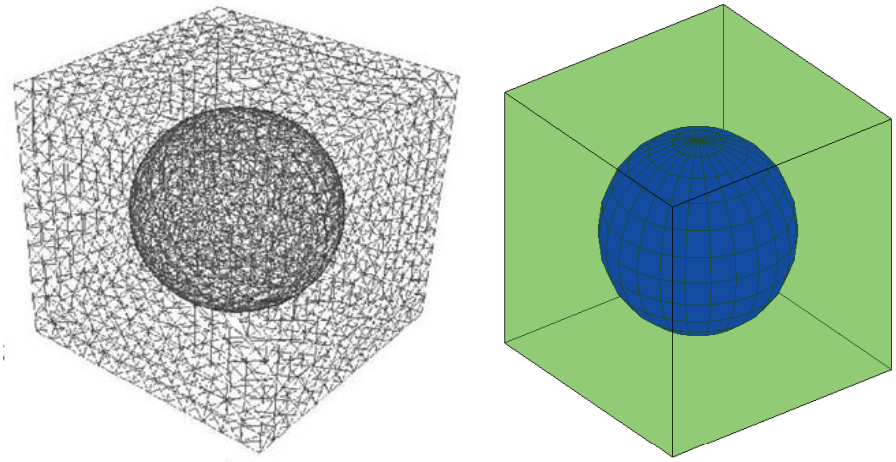

(a) (b)

Figure 12: The mesh of an Al/SiC Unit Cell model using: (a) around 76,000 ten-node tetrahedral elements with ABAQUS in the study of [Chawla, Ganesh, Wunsch (2004)]; (b) one T-Trefftz Voronoi Cell Finite Element

A uniform tensile stress of 100 MPa is applied in the x_3 direction. Both VCFEM-TT-BVP and VCFEM-TT-C are used to study the microscopic stress distribution in the RVE. However, because very similar results are obtained by these two types of VCFEM-TTs, only the results obtained by VCFEM-TT-C are shown here. The maximum principal stress in plotted in Fig. 14, and the strain energy density is shown in Fig. 15. While the inclusions are presenting a relative uniform stress state, the maximum principal stress and the strain energy density in the matrix show high concentration. To be more specific, high stress and strain energy concentration is observed near the inclusions, in the direction which is parallel to the direction of loading. On the other hand, at the locations near the inclusions, in the direction which is perpendicular to the direction of loading, very low stress values and strain energy density are observed. This gives us the idea at where damagesare more likely to initiate and develop, for materials reinforced by stiffer particles.

We also use the same RVE as shown in Fig. 13, to study porous PZT ceramic material. The RVE includes 125 spherical voids. The material properties of the matrix material are: $E = 165GPa, v = 0.22$. Only the results obtained by VCFEM-TT-C are shown here. The maximum principal stress in plotted in Fig. 16, and the strain energy density is shown in Fig. 17. The stress and energy density concentration is showing a different pattern as the Al/SiC material, of which SiC particles are stiffer

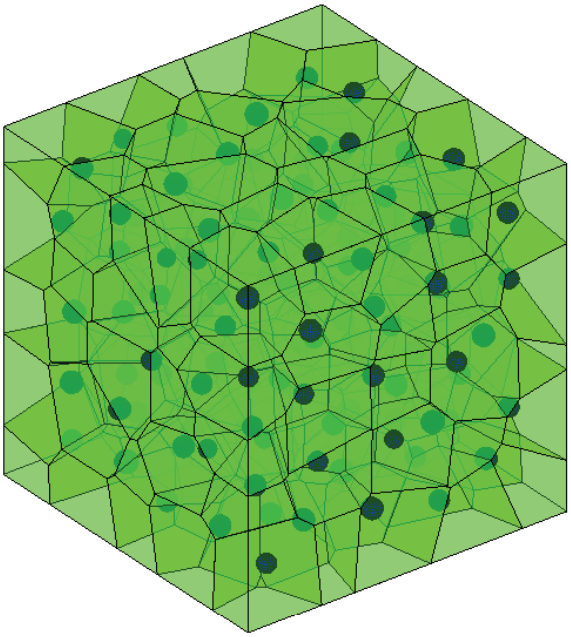

Figure 13: A RVE with 125 spherical inclusions/voids

inclusions.For PZT material with spherical pores, high stress and strain energy concentration is observed near the cavities, in the direction which is perpendicular to the direction of loading. On the other hand, at the locations near the cavities, in the direction which is parallel to the direction of loading, very low stress values and strain energy density are observed. This gives us the idea at where damage are more likely to initiate and develop for porous materials.

7 Conclusions

Three-dimensional T-Trefftz Voroni Cell Finite Elements (VCFEM-TTs) without inclusions/voids, or with spherical inclusions/voids, are developed. For each element, a compatible displacement field along the element outer-boundaryis assumed, with Barycentric coordinates as nodal shape functions. Independent displacement fieldsin the elementare assumed ascharacteristic-length-scaled T-Trefftz trial functions. Papkovich-Neuber solution is used to contruct the T-Trefftz trial

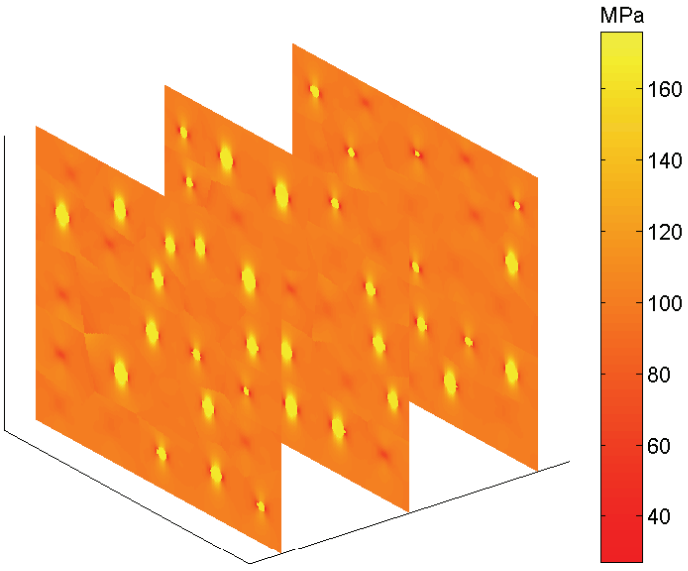

Figure 14: Distribution of maximum principal stress in the RVE of Al/SiC material modeled by 125 VCFEM-TT-Cs, each element includes a spherical inclusion

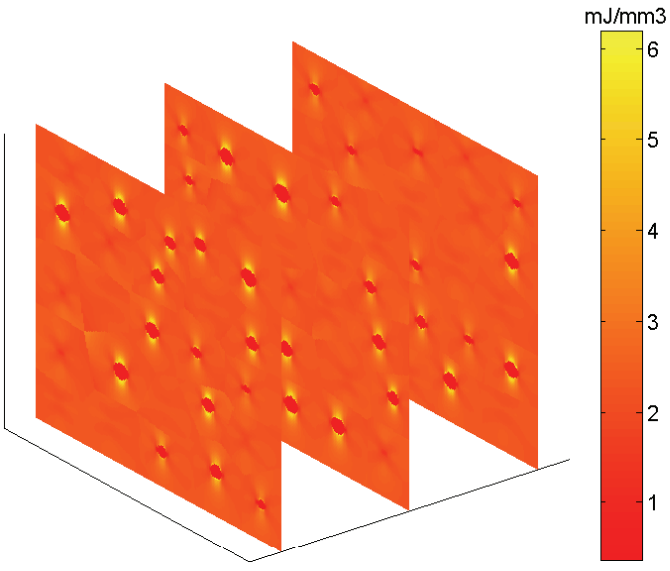

Figure 15: Distribution of strain energy density in the RVE of Al/SiC material modeled by 125 VCFEM-TT-Cs, each element includes a spherical inclusion

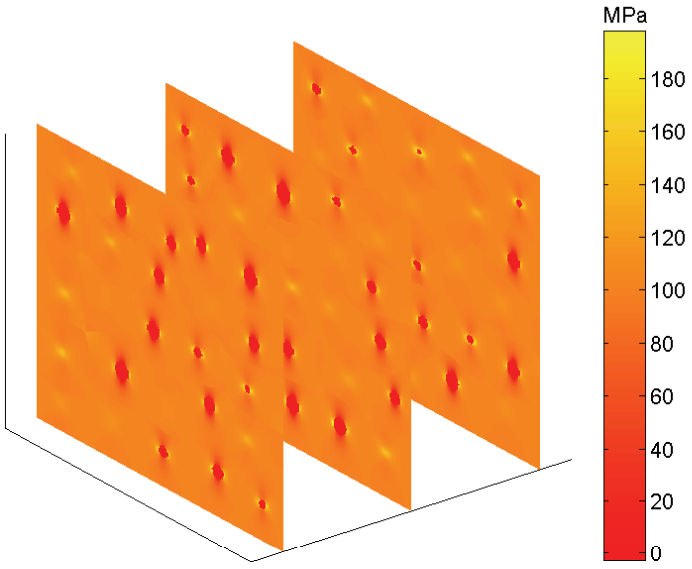

Figure 16: Distribution of maximum principal stress in the RVE of porous PZT ceramic material modeled by 125 VCFEM-TT-Cs, each element includes a spherical void

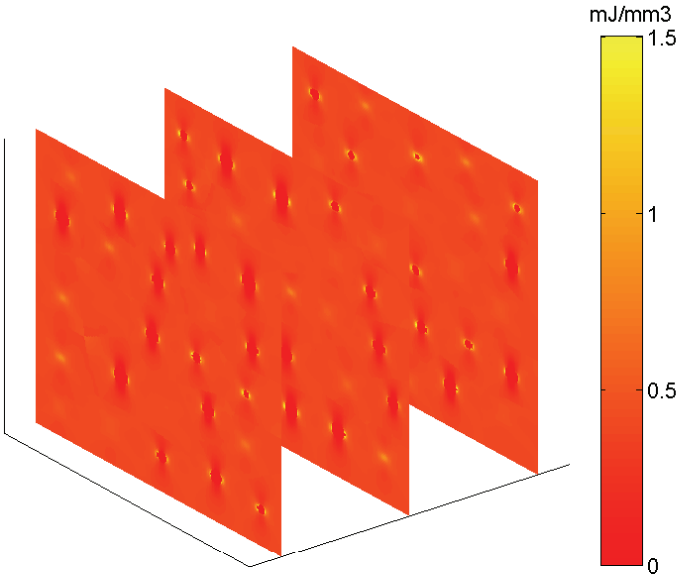

Figure 17: Distribution of strain energy densityin the RVE of porous PZT ceramic material modeled by 125 VCFEM-TT-Cs, each element includes a spherical void

displacement fields. The Papkovich-Neuber potentials are linear combinations of spherical harmonics. Two approaches are used alternatively to develop element stiffness matrices. VCFEM-TT-BVP uses multi-field boundary variational principles to enforce all the conditions in a variational sense. VCFEM-TT-C uses the collocation method to relate independently assumed displacement fields to nodal displacements, and develop finite element equations based on a primitive-field boundary variational principle.

Through numerical examples, we demonstrate thatVCFEM-TTs developed in this study can capture the stress concentration around spherical voids/inclusion quite accurately, and the time needed for computing each element is much less than that for the hybrid-stress version of VCFEMs in [Ghosh and Moorthy (2004)]. VCFEM-TTs developed in this study are also used to estimate the overall material properties of heterogeneous materials, as well as to compute the microscopic stress distribution. It is observed that, for composite materials with stiffer second-phase inclusions, high stress concentration in the matrix is shown near the inclusion, in the direction of which is parallel to the direction of loading. However, for materials with spherical cavities, high stress concentration is observed in the direction which is perpendicular to the direction of loading.

Because of their accuracy and efficiency, we consider that the 3D Voronoi Cell Finite Elements developed in this study are suitable for micromechanical modeling of heterogeneous materials. We also point out that, the process of reducing ellipsoidal coordinates/harmonics to spherical ones in the limiting case cannot work smoothly, which was contrarily presented in an ambiguous way in [Ghosh and Moorthy (2004)]. VCFEMs with ellipsoidal, and arbitrary shaped voids/inclusions will be presented in future studies.

Acknowledgement: This work was supported in part by the Vehicle Technology Division of the Army Research Labs, under a collaborative research agreement with University of California, Irvine (UCI), and in part by the Word Class University (WCU) program through the National Research Foundation of Korea, funded by the Ministry of Education, Science and Technology (Grant no.: R33-10049).

References

Babuska, I. (1973): The finite element method with Lagrange multipliers. *Numerische Mathematik*, vol. 20, no. 3, pp. 179-192.

Bao, G., Hutchinson, J.W., McMeeking, R.M. (1991): Particle reinforcement of ductile matrices against plastic flow and creep. Acta Metallurgica et Materialia, vol.39, no. 8, pp. 1871–1882.

Brezzi, F. (1974): On the existence, uniqueness and approximation of saddle-point problems arising from Lagrange multipliers. *Revue Française D'automatique, Informatique, Recherche Opérationnelle, Analyse Numérique*, vol. 8, no. 2, pp. 129-151.

Christman, T., Needleman, A., Suresh, S.(1989): An experimental and numerical study of deformation in metal-ceramic composites. *Acta Metallurgica*, vol.37, no. 11, pp.3029-3050.

Chawla, N., Ganesh, V.V., Wunsch, B. (1989): Three-dimensional (3D) microstructure visualization and finite element modeling of the mechanical behavior of SiC particle reinforced aluminum composites. *Scripta Materialia*, vol.51, issue. 2, pp.161-165.

Dong, L.; Atluri, S. N. (2011a): A simple procedure to develop efficient &stable hybrid/mixed elements, and Voronoi Cell Finite Elements for macro- &micromechanics. *CMC: Computers, Materials&Continua*, vol. 24, no. 1, pp.61-104.

Dong, L.; Atluri, S. N. (2011b): Development of T-Trefftz four-node quadrilateral and Voronoi Cell Finite Elements for macro- &micromechanical modeling of solids. *CMES: Computer Modeling in Engineering & Sciences*, vol.81, no. 1, pp.69-118.

Dong, L.; Atluri, S. N. (2012a): T-Trefftz Voronoi Cell Finite Elements with eastic/rigid inclusions or voids for micromechanical analysis of composite and porous materials. *CMES: Computer Modeling in Engineering & Sciences*, vol.83, no. 2, pp.183-220.

Dong, L.; Atluri, S. N. (2012b): A simple multi-source-point Trefftz method for solving direct/Inverse SHM problems of plane elasticity in arbitrary multiply-connected domains. *CMES: Computer Modeling in Engineering & Sciences*, in press.

Eshelby, J. D. (1957): The determination of the elastic field of an ellipsoidal inclusion, and Related Problems. *Proceedings of the Royal Society A*, vol.241, pp.376-396.

Ghosh, S.; Mallett, R. L. (1994): Voronoi cell finite elements. *Computers & Structures*, vol. 50, issue 1, pp. 33-46.

Ghosh, S.; Lee, K; Moorthy, S. (1995): Multiple scale analysis of heterogeneous elastic structures using homogenization theory and Voronoi cell finite element method. *International Journal of Solids and Structures*, vol. 32, issue 1, pp. 27-63.

Ghosh, S.; Lee, K; Moorthy, S. (2004): Three dimensional Voronoi cell finite element model for microstructures with ellipsoidal heterogeneties. *Computational*

Mechanics, vol. 34, no.6, pp. 510-531.

Guedes, J. M.; Kikuchi, N.(1990): Preprocessing and postprocessing for materials based on the homogenization method with adaptive finite element methods. *Computer Methods in Applied Mechanics and Engineering*, vol. 83, issue 2, pp. 143-198.

Hashin, Z., Shtrikman,S. (1963): A variational approach to the theory of the elastic behaviour of multiphase materials. *Journal of the Mechanics and Physics of Solids*, vol. 11, issue2, pp. 127-140.

Hill, R. (1965): Aself-consistent mechanics of composite materials. *Journal of the Mechanics and Physics of Solids*, vol. 13, no.4, pp. 213-222.

Hobson, E W(1931): *The Theory of Spherical and Ellipsoidal Harmonics*. Cambridge University Press.

Liu, C. S. (2007a): A modified Trefftz method for two-dimensional Laplace equation considering the domain's characteristic length. *CMES: Computer Modeling in Engineering & Sciences*, vol.21, no. 1, pp.53-65.

Liu, C. S. (2007b): An effectively modified direct Trefftz method for 2D potential problems considering the domain's characteristic length. *Engineering Analysis with Boundary Elements*, vol. 31, issue 12, pp. 983-993.

Lurie, A. I.(2005): *Theory of Elasticity*, 4^{th} edition, translated by Belyaev, Springer.

Muskhelishvili, N. I.(1954): *Some Basic Problems of the Mathematical Theory of Elasticity*, 4^{th} edition, translated by Radok, Noordhoff, Leyden, The Netherlands, 1975.

Nemat-Nasser, S., Hori, M.(1999): *Micromechanics: Overall Properties of Heterogeneous Materials*, second revised edition, North-Holland.

Pian, T. H. H. (1964): Derivation of element stiffness matrices by assumed stress distribution. *A. I. A. A. Journal*, vol. 2, pp. 1333-1336.

Punch, E. F.; Atluri, S. N. (1984): Development and testing of stable, invariant, isoparametric curvilinear 2- and 3-D hybrid-stress elements. *Computer Methods in Applied Mechanics and Engineering*, vol 47, issue 3, pp. 331-356.

Rubinstein, R.; Punch, E. F.; Atluri, S. N. (1984): An analysis of, and remedies for, kinematic modes in hybrid-stress finite elements: selection of stable, invariant stress fields. *Computer Methods in Applied Mechanics and Engineering*, vol. 38, issue 1, pp. 63-92..

Timoshenko, S. P.; Goodier, J. N. (1976): *Theory of Elasticity*, 3^{rd}edition, McGraw Hill

Wachspress, E. L. (1975): *A Rational Finite Element Basis*, Academic Press.